ISSN 1605-8607

EXPERIMENTAL AND NUMERICAL INVESTIGATION OF PLANE AIR WALL JET: AN APPLICATION TO VERTICAL REFRIGERATED DISPLAY CABINETS

Fareed Hussain MANGI*, Asif Ali MEMON**, Jean MOUREH***

ABSTRACT

Design of an energy efficient air curtain in particularly vertical refrigerated display cabinet has become a new challenge. The classical air curtain in a closed circuit is a longitudinal jet of cold air blown through a nozzle and sucked back by a longitudinal recovery arrangement. For a better understanding of the dynamics of air curtains, complex and case specific geometries for a fully stocked refrigerated display cabinet can be reasonably simplified to that of a plane air wall jet. A jet is said to be a wall jet, if it is blown near a wall, Wall jet has immense applications in refrigerated display cabinets, Jet cutting, cooling through impingement, heat insulation, inlet devices in ventilation, separation control in airfoils and film cooling of turbine, heating, ventilation and air-conditioning and various industrial applications.

This study aims to develop an experimental prototype to study the interaction between plane air jet confining cavity and a transverse cross-flow. To validate the proper working of the experimentally developed prototype (especially energy efficient air curtain), in the first step an academic configuration was studied which is plane air wall jet, where analytical solutions and experimental measures are available. In the prototype as well as for the numerical investigation, the plane air wall jet was investigated by using two different nozzles of 4cm and 2cm widths respectively through whom air is blown by the blower at 5m/s from top to bottom on a rectangular two dimensional domain of 0.4×0.5 m^2. The obtained experimental measurements, using Laser Doppler Velocitymetry (LDV), are compared to numerical results obtained by the commercial CFD code Fluent using different turbulent models and correlations proposed in the literature for the mean velocity profiles, maximum velocity decay, flow entrainment, friction coefficient and turbulence properties.

1. INTRODUCTION

Refrigerated Display Cabinet (RDC) is used since long time with the purpose to display the refrigerated foodstuffs forselling to the public. RDCs areused in supermarkets, food stores, convenience stores and other places where refrigerated or deep frozen foodstuffs are sold. In a RDC, the products are cooled by means of cold air flowing along the product. Alternatively the product may be cooled by means of contact cooling through the shelf or surface on which the product is placed. A combination of both is also employed. An air curtain is a planar jet of air with large aspect ratio having higher momentum than its surrounding air, used to separate the refrigerated foodstuffs inside the Refrigerated display case from the outside warm air having different characteristics and properties like temperature, airborne particle, relative humidity, etc, in the store. Therefore the outside warm air does not have much influence on the refrigerated foodstuffs [8], [12] and [13].

Air curtains are in use in many applications, i.e. Industrial climate control; air conditioned areas, industrial oven openings, dust and humidity control, mines, commercial entrances, cold storage (i.e. Refrigerated display cabinets), etc. Air curtains are often used in vertical directions and depending upon the application, they may be spilled through a circuit, or impinged on a surface located in the downstream of the jet. They may be isothermal orthermally conditioned depending upon the specific application [8].

The figure. 1 shows a classical air curtain view [5]. Here:

- ***H*** represents opening of the cabinet; and is longitudinal distance between nozzle outlet and mouth of recovery at suction mechanism;
- ***Lv*** represents longitudinal length corresponding to

*Laboratoire de Thermocinétique, CNRS-UMR 6607 Ecole Polytechnique - University of Nantes Rue Christian. Pauc, B.P. 50609, F-44306, Nantes cedex 3, France

**Energy and Environment Engineering Department, Quaid-e-Awam University of Engineering, Science and Technology, Nawabshah, Pakistan

***Genie des Procédés AN/Refrigeration Process Engineering (GPAN), Research Unit Cemagref Antony Paris France.

the cabinet length;

- ***B*** defines width of nozzle at origin;
- ***V1*** is the velocity at the origin in the axis of air curtain;
- ***M&1*** represents the mass flow rate of air at blower and recovery;
- ***t1*** is its temperature and x_1 is the title of fluid blown;
- Angle '***A'*** is the direction i.e. horizontal, vertical or inclination of air curtain;
- ***ta*** and x_a are the atmosphere of the store or shop;
- t_i and x_i are the internal atmosphere of the display Cabinet.

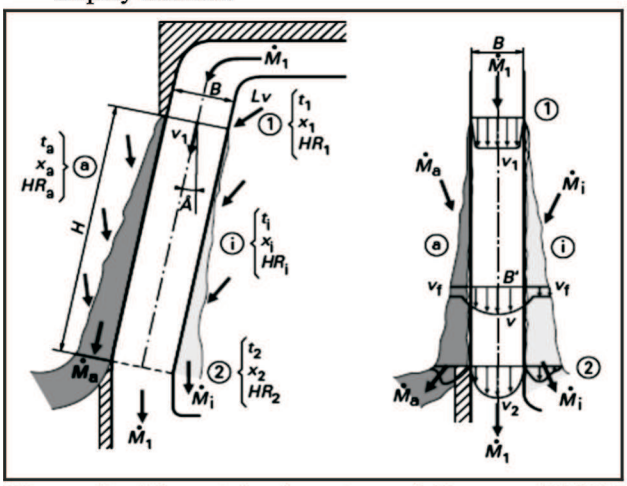

Figure 1: Air curtain (courtesy of Georges RIGOT (2009)

For a better understanding of the dynamics of air curtains, complex and case specific geometries for a fully stocked refrigerated display cabinet can be reasonably simplified to that of a plane air wall jet [4].

Jets are formed by the resultant differences of fluid pressure between two large fluid masses in the atmosphere or in confined places, particularly in the mid and upper levels. A jet is said to be a wall jet, if it is blown near a wall. In [11] a more formal definition of the wall jet given by Launder and Rodi (1981) is reported, "A shear flow directed along a wall where, by virtue of initially supplied momentum, at any station, the stream-wise velocity over some region within the shear flow exceeds that of the external stream". Because of diverse uses of plane turbulent wall jets in many applications, e.g. Jet cutting, cooling through impingement, heat insulation, inlet devices in ventilation, separation control in airfoils and film cooling of turbine, heating ventilation and air-conditioning industrial applications, researchers are very keen to evaluate wall jets from many aspects like attempts to find scaling laws and correlations [1], [6], [15] and [16].

Many experimental studies on wall jets have been carried out by various researchers e.g. starting from Förthmann (1934) and then followed by Zerbe and Selna (1946), Tuve (1953), Sigalla (1958), Myers et al (1961), Schwarz and Cosart (1961), Sforza and Herbst (1970), Sforza (1977) and Awbi (1991), and by having a good observation on these studies the formation and behaviour of wall jet, as shown in figure. 2 [14].

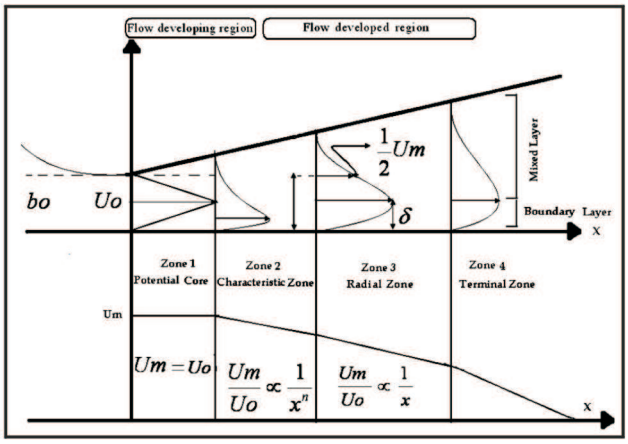

Figure 2: Characteristic Zones of Plane wall jet (courtesy of Tapsoba)

The plane wall jet can be divided into four zones in span-wise direction:
Zone 1 is called zone of potential core, here velocity remains constant in a conical and central part at the outlet of a jet. This implies that in this zone maximum velocity is equal to the velocity at inlet.

$$U_m = U_o \quad (1)$$

In zone 2, flow is developed in the perpendicular direction at the wall and can be distinguished in two layers [18] and [19]. The layer near the wall is known as boundary layer, and the layer formed on the side of air is known as mixed layer. In this zone, axial velocity decreases gradually according to the behaviour law:

$$\frac{U_m}{U_o} = \frac{1}{x^n} \qquad (2)$$

Zone 3 is known as radial zone, because of its semi-circular velocity profile. This is characterized by a high turbulent flux, and the maximum velocity in this zone is inversely proportional to the axial distance:

$$\frac{U_m}{U_o} \propto \frac{1}{x} \qquad (3)$$

Zone 4is said to be terminal zone.It is a zone of rapid diffusion in which velocity is relatively weak and tends to zero. Wall jet growth is about 0.7 times that of the free jet [15].There are also some empirical equations for the wall jet growth proposed in the literature [17].

This study aims to develop an experimental prototype to study the interaction between plane air jet confining cavity and a transverse cross-flow. To validate the proper working of the experimentally developed prototype (especially energy efficient air curtain), in the first step, an academic configuration was studied which is plane air wall jet, where analytical solutions and experimental measures are available. In the prototype as well as for the numerical investigation, the plane air wall jet was investigated by using two different nozzles of 4cm and 2cm widths respectively through whom air is blown by the blower at 5m/s from top to bottom on a rectangular two dimensional domain of $0.4 \times 0.5 m^2$. The obtained experimental measurements, using Laser Doppler Velocitymetry (LDV), are compared to numerical results obtained by the commercial CFD code Fluent using different turbulent models and correlations proposed in the literature for the mean velocity profiles, maximum velocity decay, flow entrainment, friction coefficient and turbulence properties. This paper is organized as follows: in the Section 2 experimental set up and problem description are described, Section 3 is devoted to discuss the results and discussions, Section 4 expresses the conclusion and future prospective.

2. EXPERIMENTAL SETUP AND PROBLEM DESCRIPTION

An overall view of the experimental set up is shown in Figure 3. This consists of a prototype made up of Plexiglas, usage of Plexiglas permits flow visualization of the physically studied domain and also it permits laser penetration to capture the seeded particles on the flow, a centrifugal blower through which air is blown from the top to the bottom (i.e. vertically) of the prototype, an arrangement to accommodate the honeycombs and grills with different sizes of holes in a rectangular box through which turbulence intensity is minimized and a smooth, regular and less distribution of turbulence intensity at the nozzle exit is achieved, a nozzle with width of either 4cm or 2cm is installed vertically (as we are interested here in vertical top to down flow), the configuration which is adjustable for testing wall jet as well as cavity flow (this is made possible with a glass wall which can be adjusted according to our requirements) to analyse the air jet, and an air recovery system through which recirculation is made possible, an arrangement through which oil is stored to generate seeded particles during acquisitions, and also a flow meter apparatus is installed to check the inlet conditions (i.e. velocity and flow) before starting acquisition. Wall jet is obtained by placing a wall of glass at the nozzle exit as shown in figure 3, two types of nozzles having different width (i.e. 4cm and 2cm) were used to observe wall jet while air is blown vertically from top to bottom and it is sucked back and therefore it is re-circulated. All measurements are taken by using Laser Doppler velocitymetry (LDV), with different positions on X an Y axis.

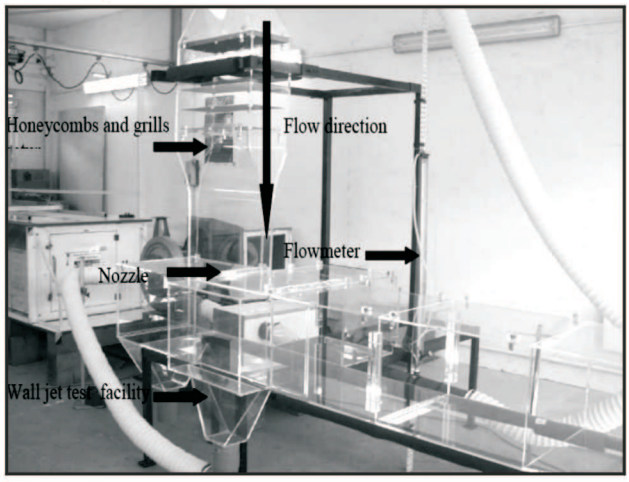

Figure 3: Prototype

2.1. GRILLS AND HONEYCOMBS ARRANGEMENT

An arrangement of grills and Honeycombs with different sizes of holes in a rectangular box is made before the nozzle inlet. Purpose of this arrangement is to reduce the turbulence intensity further more with this we may get a smooth, regular and less turbulent flow with minimum fluctuation of velocity at nozzle inlet. To select the better setup, various configurations of

different grills have diameters of holes 4.8mm, 3.2mm, 2.3mm, 1.7mm and 1.2mm and honeycombs having diameter of holes 3mm were tested to observe the turbulence intensities. The configurations were tested with measuring velocity profiles of wall jet with nozzle width of 2cm. Arrangements of grills and honeycombs in a rectangular box before nozzle inlet are given according to their placement from top to bottom in the table 1:

Table 1: Tested Configurations of Honeycombs and grills arrangement

SNo:	1st Configuration	2nd Configuration	3rd Configuration	4th Configuration	5th Configuration
01	Honeycomb (φ=3mm)	Honeycomb (φ=3mm)	Grill (φ =1.2 mm)	Honeycomb (φ=3mm)	Honeycomb (φ=3mm)
02	Grill (φ =4.8mm)	Honeycomb (φ=3mm)	Honeycomb (φ=3mm)	Honeycomb (φ=3mm)	Grill (φ =4.8mm)
03	Grill (φ =2.3 mm)	Grill (φ =3.2 mm)	Honeycomb (φ=3mm)	Honeycomb (φ=3mm)	Grill (φ =3.2 mm)
04	Grill (φ =1.7 mm)	Grill (φ =1.7 mm)	Grill (φ =2.3 mm)	Grill (φ =2.3 mm)	Grill (φ =2.3 mm)
05	Gill (φ =1.2 mm)	Gill (φ =1.2 mm)	Grill (φ =1.7 mm)	Grill (φ =1.7 mm)	Grill (φ =1.7 mm)

Comparisons of turbulent intensity obtained are shown in figure 4; the turbulence intensity changes with changing in placements of grills with different sizes of holes and honeycombs. As it is obvious entrainment is responsible for most of refrigerating load in display cases, so it is possible to decrease amount of entrainment in air curtain therefore one can design an air curtain which has less fluctuation in velocity thus less turbulence intensity, keeping in view this importance different arrangements of honeycombs and grills were checked by using Laser Doppler velocitymetry (LDV).

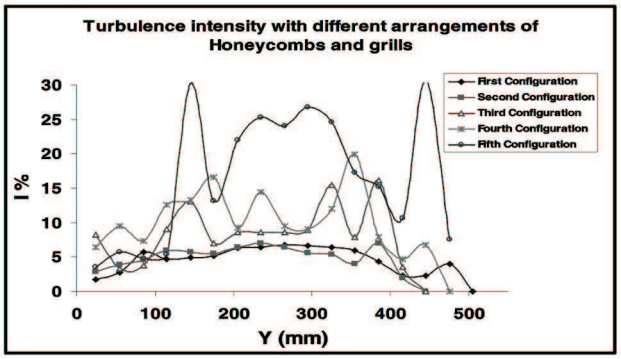

Figure 4: Turbulence intensity function of placement of honeycombs and grills

Figure 4, shows with first configuration the turbulence intensity obtained is fluctuating between 0% and 5%, but it is approximately constant between 200mm and 350mm along the y-positions. Second configuration represents turbulence intensity between 0% and 5%, and with this configuration it is observed that turbulence intensity fluctuate span wise along y-positions, while the other three configurations (i.e. 3rd, 4th and 5th) predict turbulence intensity above the limit (i.e. 10% which is affordable), Therefore configuration was selected for our experimental work.

3. RESULTS AND DISCUSSION

As described in earlier section, that 2D wall jet configurations with two different nozzles with width (b_0) of 4 cm and 2 cm respectively were analyzed. For 4 cm configuration we used two different types of meshes i.e. coarse mesh and fine mesh which are generated with the GAMBIT software. The commercial software FLUENT was used as solver. The coarse mesh simulations standard wall function was selected. While for the fine mesh enhanced wall treatment was used. To validate the numerical results using LDV in the prototype, nozzles of width (b_0) 4 cm and 2 cm respectively were used.

3.1 BOUNDARY CONDITIONS

To investigate numerically the configuration as shown in *figure 5* the boundary conditions are defined according to the physical problem description. The right vertical and left vertical sidesof $0.4 \times 0.5 m^2$ domain are defined as walls.

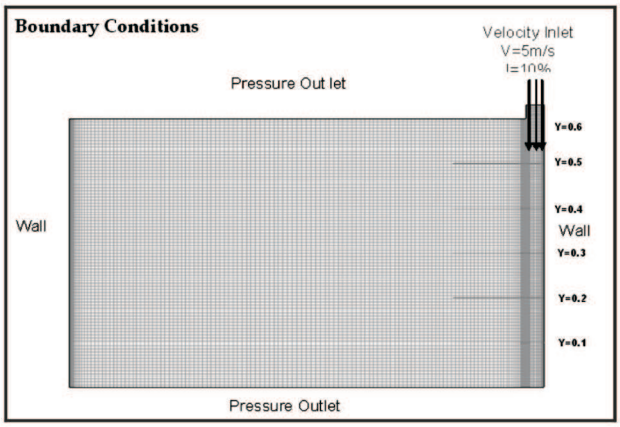

Figure 5: Boundary conditions in 2D wall jet configuration

As direction of jet is from top to bottom so some lines are marked to observe flow characteristics from flow developing region (i.e. Potential core) to the flow development region. To obtain free wall jet, upper and lower sides of the 2D configuration are considered as pressure outlets. To avoid recirculation and vortex formation, at the bottom near the jet and for the original nature of the jet, a very small pressure difference between two pressure outlets, which we have supposed here as ΔP=0.1 Pa. Importance of this pressure difference is illustrated in figure 6 and 7.

In figure 6 with ΔP=0, recirculation in the flow path lines observed which does not resemble the wall jet characteristics.

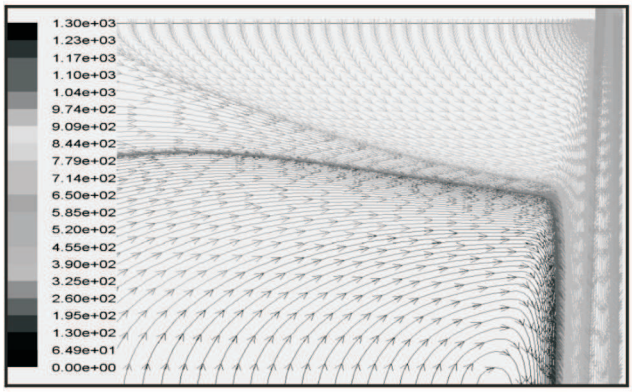

Figure 6: Flow path lines with ΔP=0 Pa

After applying $\Delta P=0.1Pa$, figure7shows that there is no more recirculation in the jet.

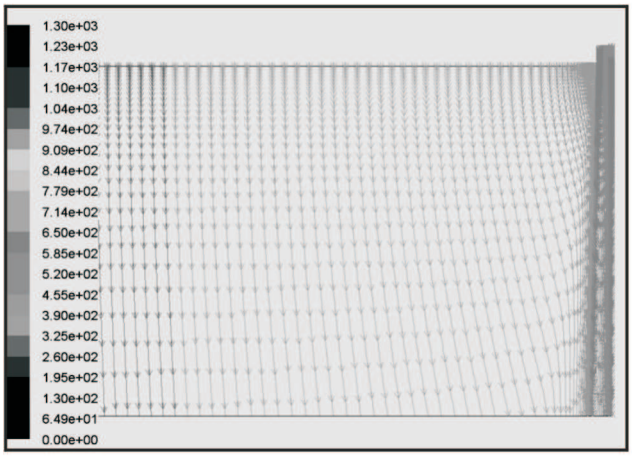

Figure 7: Flow path lines with ΔP=0.1Pa

3.2. MESH

Two types of meshes were generated i.e. Coarse Mesh and Fine mesh by using commercial software GAMBIT.

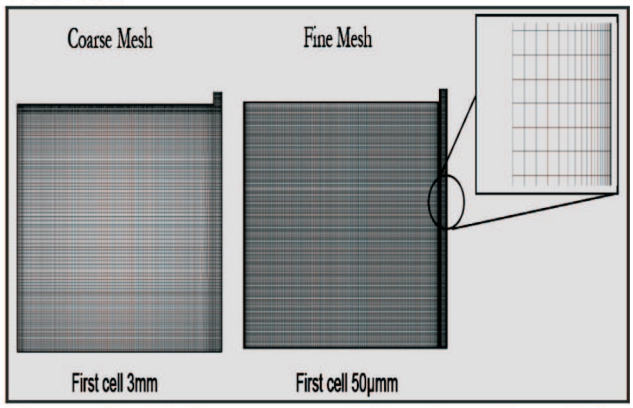

Figure 8: Mesh types used for the 2D wall jet configuration

Coarse mesh was generated to obtain global information of the expected results, while the Fine mesh was generated to obtain specific and detailed information. Coarse mesh was generated by using first cell 3 mm, and total number of cells is 15230, the fine mesh for 4cm nozzle width configuration was generated first cell as 50μmm and total number of cells are 38904, and for the fine mesh using 2cm nozzle width configuration mesh was generated by using first cell as 50 μm first cell and total number of cells are 89000. The meshes are shown in the figure 8. To validate these meshes it is very important to calculate Y^+ at wall, to confirm either it respects the numerical recommendations or not, which is shown in the figure (9 a) and (9b).In figure 9a we can observe that the value of Y^+ increases with respect to distance from 2.5 to 36 maximum while for the coarse mesh it is affordable up to 100. Similarly while having a look on figure 9b the value of Y^+ increases with respect to distance and it lies between 0.9 and 1.3 maximum while for the fine mesh it is affordable up to 5.

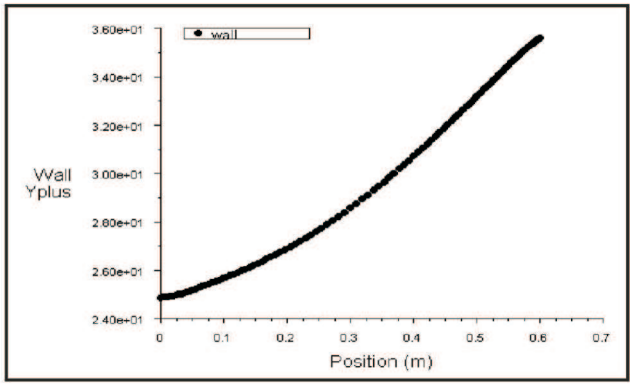

Figure 9a: y plus for coarse mesh

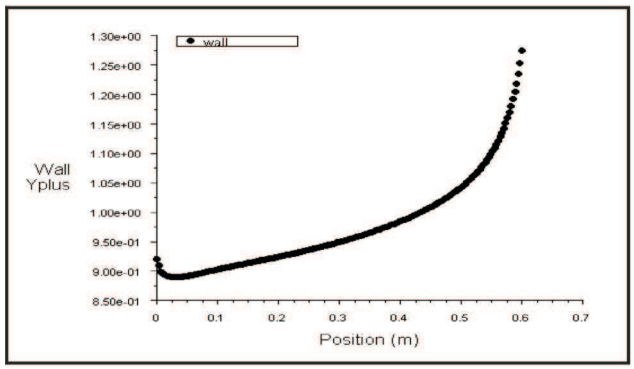

Figure 9b: y plus for fine mesh

3.3. COMPARISONS OF CONFIGURATION HAVING 4 CM NOZZLE WIDTH (COARSE MESH)

3.3.1. MEAN VELOCITY PROFILES (COARSE MESH:)

When the wall jet develops, its velocity is reduced and it expands normal to the wall. The behaviour of maximum velocity (U_m) and half-width (b) is used to investigate the decrease in the velocity and normal expansion to the wall. A good agreement between the mean velocity profiles measured in this work (i.e. both experimentally and numerically) and those obtained by [3] also reported by [18]. The velocity profiles of both configurations (i.e. with nozzle width 4 cm and 2 cm respectively) obtained by FLUENT using six different turbulent models to validate with the LDV results are plotted at different Y-positions. Figure 10a represents velocity profile at y-position = *2.5 cm* therefore at an aspect ratio (*Y/b=0.625*) which is just *2.5 cm* below the nozzle exit. Rectangular shape velocity profiles are due to a fact that at this point flow is not developed, this location is potential core. Figure 10b illustrates that how jet starts developing and the rectangular shape of velocity profiles begins to change in semi-circular shape. The numerical results are in good agreement with the LDV results, Reynolds shear stress model (RSM) and Standard K-epsilon (SKE), and are much closer to the experimental results than other turbulent models, and give relative error less than 5%. Figure 10c illustrates velocity profiles of developed region and we have obtained almost identical curves of LDV results as well as the numerical results. Figure 10d also shows a good agreement in the curves of numerical and LDV results. The comparison with data in [3] is also made, the difference between data of [3] and our experimental data is due to the difference between aspectratio. Aspect ratio at this point as Y/b = 8.625, while in the [3] minimum aspect ratio of 21.7 is used. All models seem to be in good agreement with experiments performed using with Laser Doppler Velocitymetry (LDV).

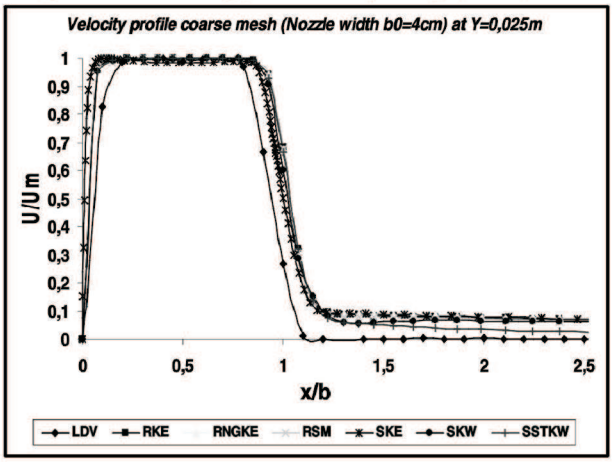

Figure 10a: Velocity profiles at potential core

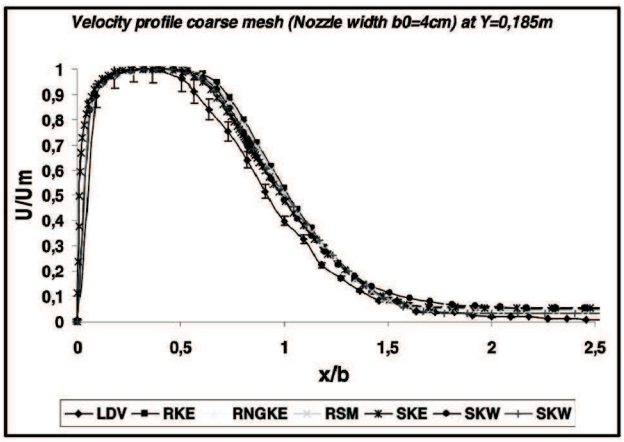

Figure 10b: Velocity profiles (Coarse mesh) at y=18.5 cm

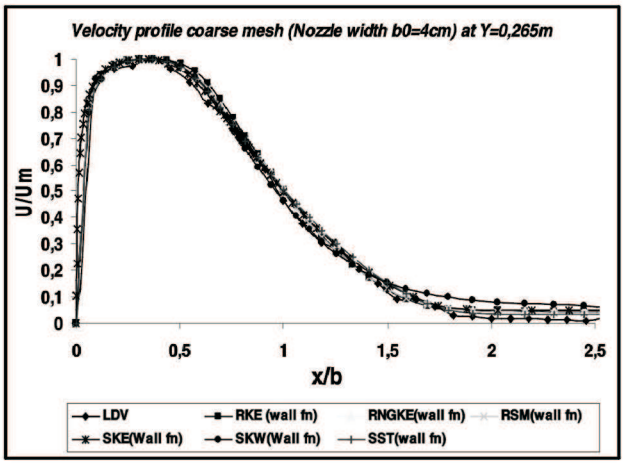

Figure 10c: Velocity profiles (Coarse mesh) at y=26.5 cm

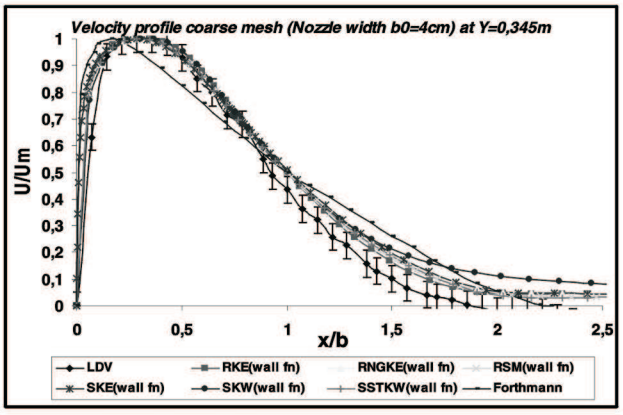

Figure 10d: Velocity profiles (Coarse mesh) at y=34.5cm

3.3.2 MAXIMUM VELOCITY DECAY (COARSE MESH)

Figure 11 illustrates the maximum velocity decay at y-positions.Results are compared with an analytical equation for developed flow which is proposed in [15].

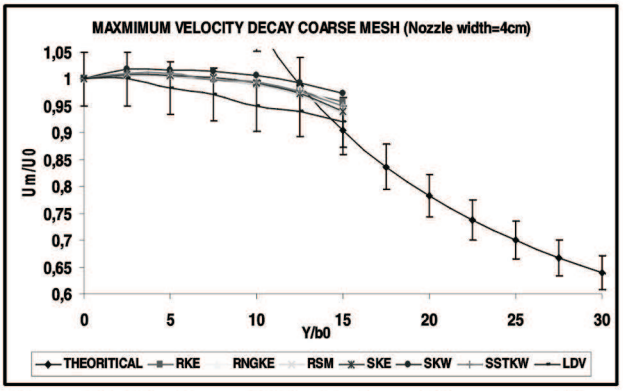

Figure 11: Maximum Velocity decay (Coarse mesh)

$$\frac{Um}{U_0} = 3.5/\sqrt{x/b_0} \text{ For } \frac{x}{b_0} \text{ up to } 100 \qquad (4$$

Similarity in curves is observed according to the correlation proposed. However, due to small aspect ratio (y/b) of 15 in our case, it could not be compared for larger aspect ratios. Reynolds shear stress (RSM) and Standard K-Epsilon turbulence models have good agreement with both LDV within five percentof standard deviation.

3.3.3. JET ENTRAINMENT (COARSE MESH):

Jet entrainment is compared with an equation proposed in[18],

$$\frac{Q}{Q_0} = \left[1 + 0.04\,\frac{\bar{x}}{b_0} + 0.0046\left(\frac{\bar{x}}{b_0}\right)^{0.8}\right] \qquad (5$$

In figure 12 both numerical and LDV results show better accordance with the equation. All numerical models show good agreement with the LDV results with 5% of maximum deviation, where Reynolds shear stress model (RSM) is closest to LDV results.

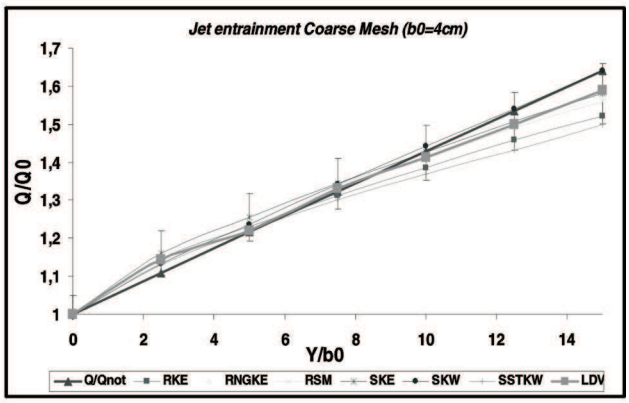

Figure 12: Jet entrainment (Coarsemesh)

Considering the anisotropy of the turbulence, RSM is an appropriate model for predicting the flow structure precisely.

3.3.4.. COEFFICIENT OF FRICTION (COARSE MESH):

An equation given by Sigalla (1958) is reported in [15],

$$C_f^i = \frac{\tau_0}{(\rho U_0^2/2)} \approx \frac{0.0565}{(Um\delta/\upsilon)^{1/4}} \qquad (6$$

In figure 13 coefficients of friction obtained numerically are compared with the equation (6); all turbulent models show good agreement with it.It was not possible to determine the coefficient of friction experimentally because with LDV it is not possible to measure velocity at few μm of wall.

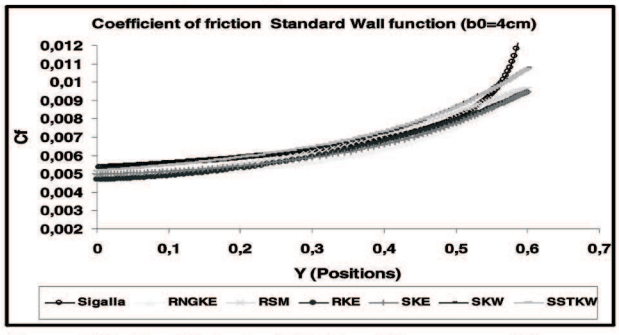

Figure 13: Coefficient of friction (Coarse mesh)

3.4. COMPARISONS OF CONFIGURATION HAVING 4 CM NOZZLE WIDTH (FINE MESH)

3.4.1. MEAN VELOCITY PROFILES (FINE MESH)

Mean velocity profiles are compared for a refined mesh in a similar way as previous. The numerical results are compared with the same LDV results with whomthe results were compared for the coarse mesh.Figure 14*a*presents velocity profile at y-position=0,025, same position on which we have already discussed the coarse mesh case. Good agreement between numerical and experimental results was observed.With a changed mesh some variations wereseen in the Standard K-Omega turbulent model, where velocity does not diminish according to experimental and other turbulent models.Figure 14b this velocity profile shows some rectangular and semi-circular mixed shapes, because after the potential core jet starts to develop. At this y-position a good agreement between numerical results and experimental results is also observed, except standard K-Omega. Figure 14c also shows the velocity profile at developed flow. LDV and numerical results coincide with each other, except standard K-Omega which shows some agreement while velocity increases but becomes constant at $U/U_m = 3$. In figure 14d, data given in [3] was also added to see the similarity in curves. As we have already discussed that the difference in profiles is due to large aspect ratio which was used by Förthmann in 1934, otherwise both numerical and experimental results coincide with each other except the standard K-Omega turbulent model.

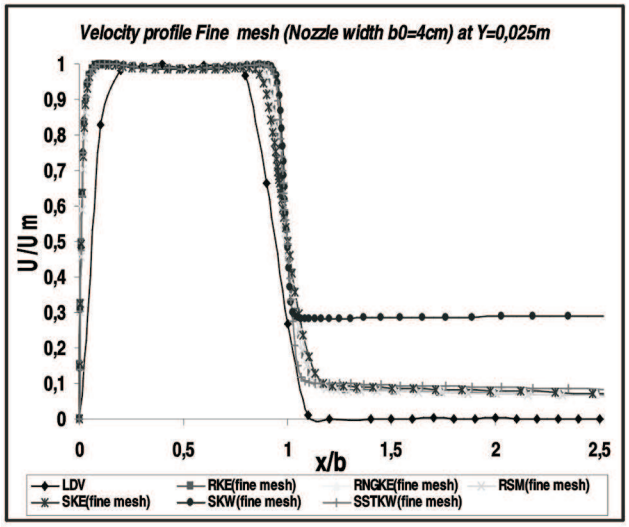

Figure 14 a: Velocity profiles at potential core (Fine mesh)

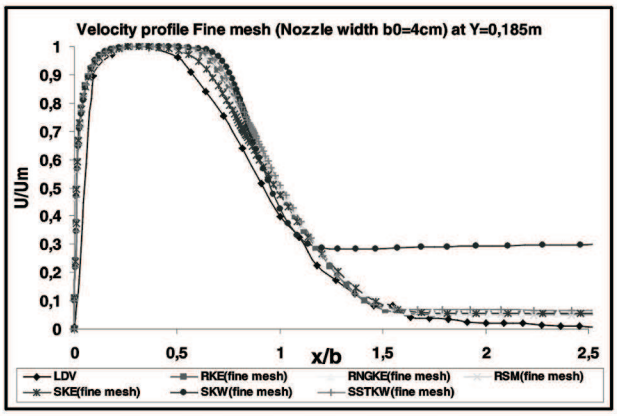

Figure 14b: Velocity profiles (Fine mesh) at y=18.5 cm

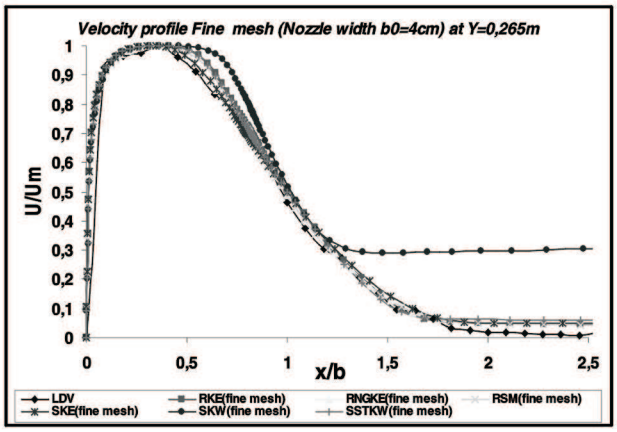

Figure 14c: Velocity profiles (Fine mesh) at y=26.5 cm

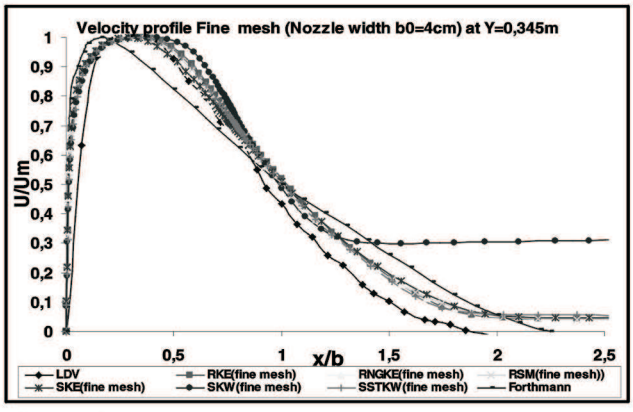

Figure 14d: Velocity profiles (Fine mesh) at y=34.5 cm

3.4.2. MAXIMUM VELOCITY DECAY (FINE MESH)

Figure 15, which show a good agreement in maximum velocity decay of experimental and numerical results with equation (4). SKE, RSM and Standard K Omega turbulent models are closer to the LDV results.

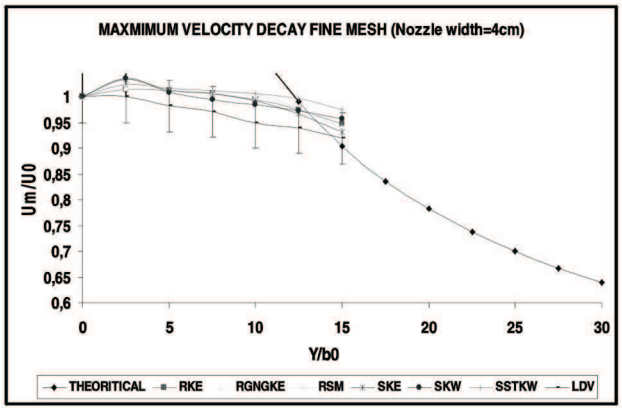

Figure 15: Maximum Velocity decay (Fine mesh)

3.4.3. JET ENTRAINMENT (FINE MESH)

Figure 16 illustrates numerically obtained jet entrainment compared with the equation (5) and LDV results. A good agreement wasobserved between all turbulent models and LDV results with maximum 5% standard deviation.

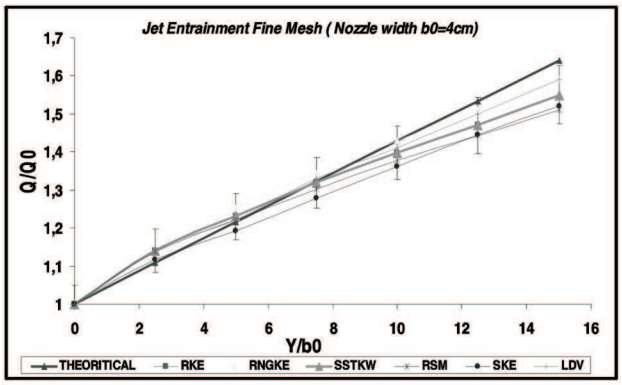

Figure 16: Jet entrainment (Fine mesh)

3.4.4 COEFFICIENT OF FRICTION (FINE MESH):

Figure 17 illustrates the comparison between the equation (6) and numerical curves of coefficient of friction. RSM, RNGKE and SKE turbulent models are much closer to the theoretical curve.

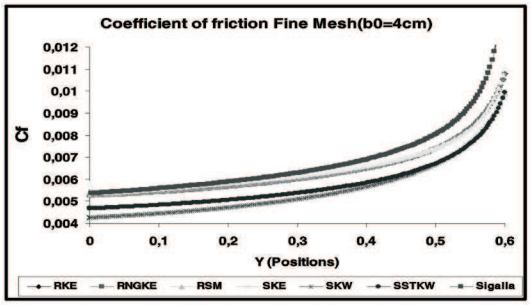

Figure 17: Coefficient of friction (Fine mesh)

3.4.5. Y-PLUS

Velocity distributions in the boundary layer region of plane wall jet are plotted in figure 5.15. This graph is drawn at y-position= 0.3 m, where from $Y^{+}=10$ the curves obey the log law

$$\frac{U}{U_{*}} = 5.6\log\left(\frac{yU_{*}}{\upsilon}\right) + 4.9$$ and from $Y^{+}=1$ to $Y^{+}=10$the curves are concave in shape [9] and [10].

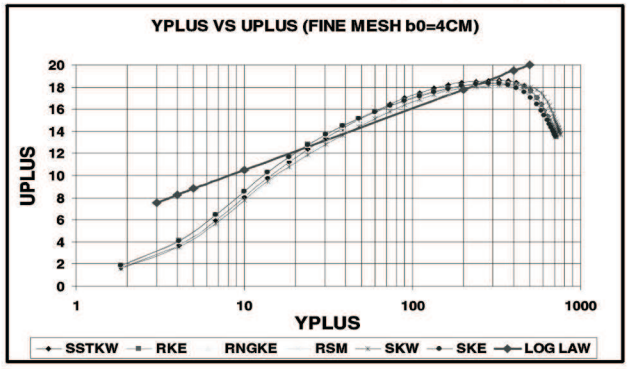

Figure 18: Y^{+} Vs U^{+} (Fine Mesh nozzle width b_0= 4cm)

Turbulent models RSM, SKE are much closer than the other models to the line of log law.

3.5. COMPARISONS OF CONFIGURATION HAVING 2 CM NOZZLE WIDTH (FINE MESH)

3.5.1. MEAN VELOCITY PROFILES:

For the configuration of 2 cm nozzle width the same comparisons were also made. Figure 19 shows behaviour of velocity at y-position=0.345m. Thisprofile is at flow developed region and all turbulent models have shown good agreement with LDV results as well as with data given in [4].

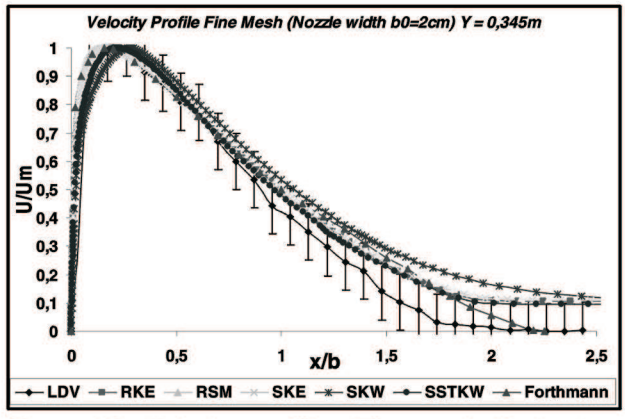

Figure 19: Velocity profiles (Fine mesh b0=2cm) at y=34.5 cm

SKE and RSM are closer than the other turbulent models to the LDV results.RSM model improves the prediction of the velocity level in the jet and in some special cases it may influence the entire flow in the occupied zone [2].

3.5.2. MAXIMUM VELOCITY DECAY:

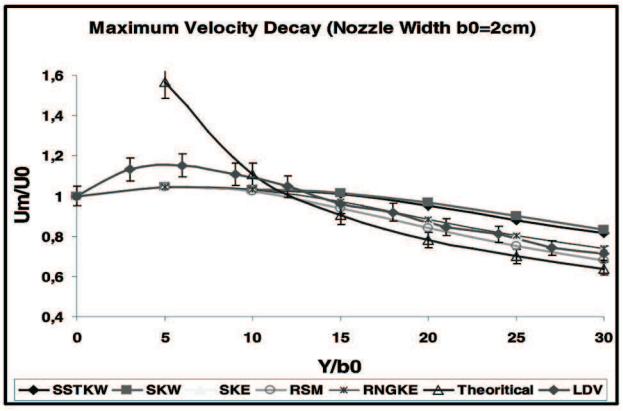

Figure 20: Maximum Velocity decay (Fine Mesh b_0 =2cm)

Like previous cases, maximum velocity decay curve is found to be in accordance with the equation (4) and LDV results. Figure 20 shows the maximum velocity decay curve of configuration having 2 cm nozzle width. All turbulent models are found to be in good accordance with the equation (4) and LDV curves. LDV curve is between RSM and SKE curves.

3.5.3. JET ENTRAINMENT

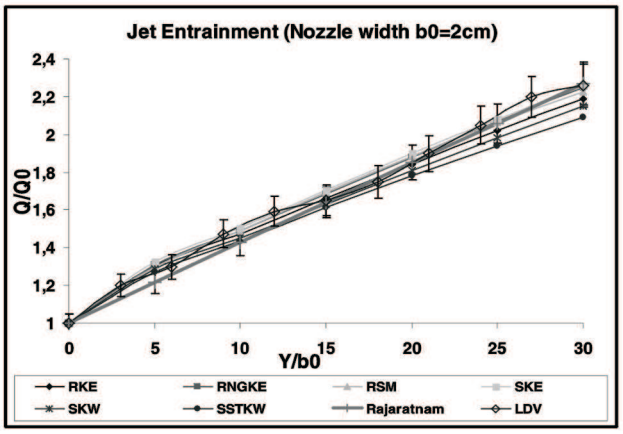

Figure 21: Jet Entrainment (Fine Mesh nozzle width b_0 =2cm)

Figure 21 illustrates the comparison between equation (5), LDV results and numerical results for the Jet entrainment. A good agreement was observed between all turbulent models and LDV results with maximum 5% of standard deviation.

3.5.4. COEFFICIENT OF FRICTION:

Figure 22all turbulent models follow curve of the equation (6) with a slight difference from nozzle exit. This may be due to the fact that all theoretical equations are valid for developed flow regions.

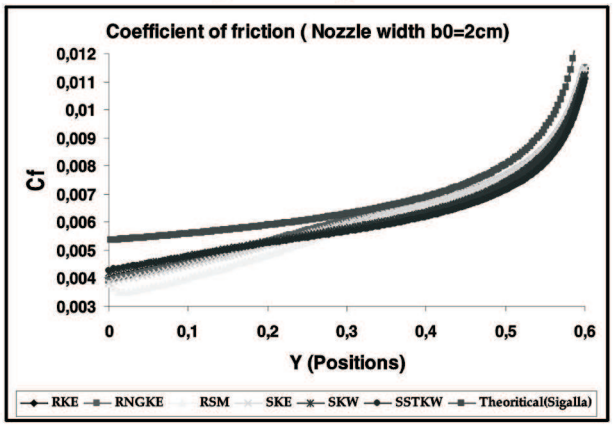

Figure 22: Coefficient of friction (Fine Mesh nozzle width b_0 =2cm)

RNGKE, RSM and SKE are very close to the theoretical curve in flow developed region.

3.5.5. Y-PLUS

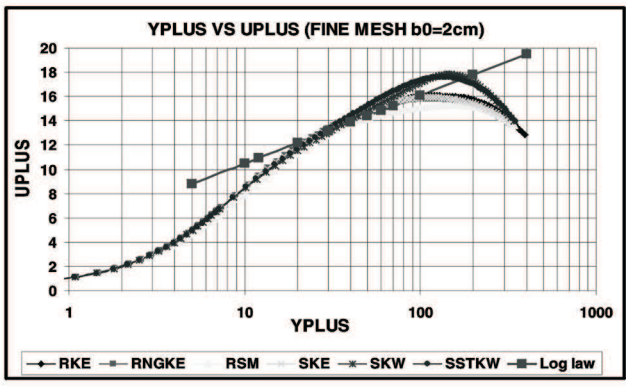

Figure 23: Y^+ Vs U^+ (Fine Mesh nozzle width b_0= 2cm)

Velocity distributions in boundary layer region of plane wall jet are plotted in figure 23. Turbulent models SKW and SSTKW are over predicting the log law, while the other four turbulent models have good agreement with the log law line.

4. CONCLUSION AND FUTURE PROSPECTIVE

The study on wall jet was performed on two different configurations of nozzle width 4cm and 2cm respectively. With the obtained results of plane wall jet tested in prototype by using Laser Doppler velocitymetry (LDV) and analytical results were used to validate numerical results of turbulent models obtained by using a commercial code FLUENT. A good accordance was obtained between experimental, numerical and analytical results by comparing their velocity profile, maximum velocity decay curves, amount of jet entrainments, coefficients of friction curves and velocity distributions in boundary layer regions. From the numerical point of view it was also concluded that use of fine mesh gives more accurate results than the coarse mesh. As for as turbulent models investigated numerically by using commercial code FLUENT almost found with good agreement with experimental and analytical results. The turbulent models SKE and Reynolds shear stress model (RSM) were in better accordance with the LDV results as compared to other four models.

Experiments are performed to analyze cavity flow with varying degree of cavities resembling vertical display cabinets with LDV and PIV techniques to validate numerical simulations. Moreover this prototype is designed to observe the cross-flow characteristics (which will be tested in near future) applied to RDC. Therefore, another blower will be blown horizontally to see the perturbation behaviour with the vertically blown air, so called air curtain. The objective is to decrease the entrainment rate which is a main factor influencing on refrigeration load. This may be helpful for designing an energy efficient air curtain.

REFERENCES

[1] AméniMokini, HatimMhiri, Georges Le Palec, Philippe Bournot., (2008) *Numerical study of vertical wall jets:* International Journal of Fluid and Thermal Engineering 1:4 2008.

[2] A. Schälin and P.V. Nielsen, (2004), Impact of turbulence anisotropy near walls in room airflow, *Indoor Air***14** (2004), pp. 159–168.

[3] E. Förthmann, Überturbulentestrahlaus breitung, *Ingenieur-Arch***5** (1) (1934), pp. 42–54 translated as: Turbulent jet expansion. National Advisory Committee for Aeronautics, Technical Memorandum, No. 789, National Aeronautics and Space Administration, USA, 1936.

[4] E. Loth, P. Bhattacharjee., (2004), *Simulations of laminar and transitional cold wall jets.*International Journal of Heat and Fluid Flow 25 (2004) 32–43.

[5] Georges RIGOT., (2009), *Meubles frigorifiques de vente*, Techniques de l'Ingénieur, traité Génie énergétique, *(Institut français du froid industriel IFFI)Cemagref Dossier.*

[6] G. I. Barenblatt, A. J. Chorin, and V. M. Prostokishin; (2005),*The turbulent wall jet: A triple-layered structure and incomplete similarity*

[7] Hazim B. Awbi., (1991), *Ventilation of Buildings.* Second editionSpon London EC4P 4EE.

[8] Homayun K. Navaz, Brenda S. Henderson, RaminFaramarzi, Ahmad Pourmovahed, Frederic Taugwalder, (2005), *Jet entrainment rate in air curtain of open refrigerated display cases.* International Journal of Refrigeration 28 :p 267–275.

[9] http://www.cfd-online.com.

[10] Introductory FLUENT notes, FLUENT v6.3(2006), www.fluentusers.com.

[11] J.G. Eriksson, R.I. Karlsson, J. Persson., (1998), *An experimental study of a two-dimensional plane turbulent wall jet.* Experiments in FluidsVolume 25, p 50-60.

[12] Ke-zhi Yu, Guo-liangDing ,Tian-ji Chen, (2007),*Simulation of air curtains for vertical display cases with a two-fluid model.*Applied Thermal Engineering 27 (2007) 2583–2591.

[13] M. Amin, H.K. Navaz, D. Dabiri& R. Faramarzi, (2006), *Air curtains of open refrigerated display cases revisited: a new technique for infiltration ratemeasurements.*

[14] MitoubkietaTapsoba., (2005), Thèse *Etudes expérimentale et numérique de l'aéraulique dans un véhicule frigorifique*. Thèse à l'Institut de recherche pour l'ingénierie de l'agriculture et de l'environnement; Unité de recherche Génie des procèdes frigorifiques- Antony- France.

[15] Rajaratnam, N., (1976), *Turbulent jets*: Elsevier Publishing Co.

[16] Rajaratnam, N. and Subramanya, K., (1967), *Diffusion of rectangular wall jets in wider channels.* J. Hydraul. Res., 5:281-294.

[17] S.S Aloysius, L.C Wrobel., (2009), *Comparison of flow and Dispersion properties of free and wall turbulent jets for source dynamics characterisation.*Environmental Modelling& Software 24 (2009), p 926–937.

ISSN 1605-8607

WEB SUSCEPTIBILITIES AND THEIR PREVENTION IN PAKISTAN

Ali Raza Bhangwar, Pardeep Kumar, Adnan Ahmed

ABSTRACT

The use of Internet in Pakistan has increased dramatically over the last years. Several organizations whether they are related to government, private, education or commercial sector use websites to provide required information to their visitors/customers. However, the detail study of such websites suggests that the web developers mostly ignore the security issues and just concentrate on how to make the website attractive. Several such websites are easily vulnerable to the major web security attacks such as SQL injection, cross site request forgery, scripting and tracing, denial of service, buffer overflow, etc. This research work attempts to identify the web vulnerabilities present in Pakistani websites by using the penetration techniques, proposes a suitable solution to these vulnerabilities and presents the statistical data of several websites from different sectors in a graphical form.

1. INTRODUCTION

Many organizations in Pakistan are now using Internet to provide the required information to the public and to expand their publicity and growth. As Internet has become the backbone of the information exchange in today's world and offers new opportunities to the businesses and individuals, its utilization in Pakistan is also increasing on the daily basis.

The arrival of web 2.0 and AJAX have further significantly improved the world of Internet where the user could interact in real time. At the same time, they are susceptible to the several security vulnerabilities and have opened the new windows for the hackers. The researchers are constantly working on the security flaws and trying their best to minimize the consequences of the security flaws. Whereas the attackers are as skilled as the security experts so the attackers are also constantly working on it and finding the new ways to exploit these security flaws.

With the fast growth of Internet and the swift transition from the traditional to the web based approach, many web developers significantly ignore web application's security issues and mainly focus on developing attractive websites for the customers. In result, they develop web applications with variety of vulnerabilities, some of them are enlisted in [10] and [11]. In result of that, the malicious users always try to take advantage and exploit these vulnerabilities.

Various organizations in the world, particularly in the developed countries, are now involved in providing awareness for these vulnerabilities by publishing a list of top vulnerabilities every year and by providing their solutions and by implementing them. But in Pakistan very less attention has been paid to the web security, its vulnerabilities and implications. This paper is therefore an attempt to provide awareness and susceptibilities regarding the web security in Pakistan and their tentative solutions.

Penetration testing is the well-known method of auditing the websites for security breaches. It is basically a combined approach of knowledge, skills and experience. It analyzes the website for security breaches by attacking the website with the same analogy as the attackers do. After identifying the vulnerabilities, penetration tester provides necessary solutions to the identified vulnerabilities. This work basically uses the penetration technique to identify and then propose solution to the several web vulnerabilities.

This paper is organized as follows: Section 2 provides the detail of the penetration techniques and Section 3 presents the research methodology that has been used to identify the security vulnerabilities. Section 4 presents the different vulnerabilities that have been identified for the several websites in Pakistan. Section 5 shows the related work in the domain whereas the last Section 6 concludes the overall research work and presents some proposed recommendations.

2. SECURITY PREVENTION TECHNIQUES IN DETAIL

This section briefs the web vulnerabilities; there detail discussion is given in [1], [3] and [9]. Here we mainly focus on the prevention techniques for those security concerns. The major web vulnerabilities and their prevention techniques are given below

2.1. SQL INJECTION

Because of SQL Injection's popularity, it is the most discussed vulnerability by the different authors and they have suggested different solutions to the same vulnerability [2], [3] and [4]. We in this paper focus on code level defense. The code level defense method is the most common and efficient technique since all other defensive techniques need to use this technique at the end. One of the fundamental assumptions of SQL Injection vulnerability is the dynamic building of SQL query. The alternative method of dynamic building SQL query is to use parameterized statements [4].

2.1.1. PARAMETERIZED STATEMENT

Parameterized statements are the place holders whose value is replaced at run time. Almost every programming language now supports parameterized statement. As an example we have taken a vulnerable query as shown in Figure 1 [4], which take user's inputs and generate dynamic SQL query, and then focus is made on how to secure it with the use of parameterized statements, for readers who want to read further on prevention of SQL Injection can read article [8].

```
Username = request("username")

Password = request("password")

Sql = "SELECT * FROM users WHERE Username='"+
username + "'AND password ='"+ Password + "'"

Result = Db.Execute(Sql)

If (Result) /*suceesful login */
```

Figure 1: Vulnerable SQL Query [4].

The above mentioned query takes user input and processes it for execution without sanitizing it.

The secure version of above mentioned example with the help of parameterized statements is as given in Figure 2 [4].

```
sqlConnection con = new SqlConnection (ConnectionString);

string Sql = "SELECT  * FROM users WHERE
username=@username" + "AND password=@password";

cmd = new SqlCommand(sql, conn);

//Add parameters to SQL query

cmd.Parameters.add("@username",      // name

        SqlDbType.NVarChar,          // data type

        16);                         // length

Cmd.Parameters.Value("@username") = username; // set
parameters

Cmd.Parameters.Value("@password") = password; // to
supplied value

Reader = cmd.ExcuteReader( );
```

Figure 2: Parameterized SQL Query [4].

The parameterized statements not only provide an alternative for dynamic SQL building but also additionally checks for length and type of the input received. Username and password fields are now safe and will be checked that it contains a valid username and password and whether its type is correct along with the length. Request will be rejected if the input received will not match the required constraints.

2.1.2. INPUT VALIDATION

It's a method of analyzing the inputs the application gets against predefined set of inputs. The idea is to check all the received inputs which application might receive and process them if inputs are validated, if inputs differs from pre-defined set of inputs must be rejected. Researchers have suggested different techniques for input validation [5], [6], and [7], but the best method to sanitize inputs is to use regular expressions [7]. An example of validating inputs in C# programming is given in Figure 3 [4].

```
<asp:textbox id="username" runat="server"/>
<asp:RegularExpressionValidator id="usernameRegEx"
runat="server" ControlToValidate="user-name"
ErrorMessage="Username must contain 8-12 letters only."
ValidationExpression="^[a-zA-z]{8,12}$" />
```

Figure 3: Input Validation on .NET [4].

2.1.3. STORED PROCEDURES

Stored Procedures is a collection of statements in compiled forms within the database, it can significantly reduce the risk of SQL Injection vulnerability, as it gives restricted permission to access the data from the database. So if SQL Injection vulnerability is found, the attacker cannot change important information within the database if access permission is set properly by the developer. It may be noted that in some situations Stored Procedures alone may not protect from SQL Injection vulnerability, therefore it is best practice and suggested by Microsoft to use Parameters with Stored Procedures [16].

2.1.4. OUTPUT ENCODING

Output encoding is the process of safely handling the outputs which are about to be returned by the application in response of the request made, as it happens that sometimes the data supplied by the user will be processed by the application for output, therefore any malicious data which simply gets returned by the application for output processing can lead to potential SQL Injection. Therefore, it is necessary that whatsoever data is supplied to database must be encoded. In SQL encoding is done as: sql = sql.Replace("' '", "'' '');.

2.2. CROSS SITE SCRIPTING

Cross Site Scripting (XSS) is one of the most exploitable of all web attacks; XSS web vulnerability allows an attacker to inject a malicious code into the website which causes the visitors of the website to be the ultimate victim of the attacker. It was first observed by the CERT and stood 2nd position at OWASP for 2010 list. XSS vulnerability has victimized approximately 80.5% of all web attacks published by Symantec in 2008 [17]. There are two types of XSS vulnerability as given below.

2.2.1. PERSISTENT CROSS SITE SCRIPTING

Persistent XSS is sometimes called stored XSS, this vulnerability gives the attacker a chance to upload his data at the server and will be exploited when other users visit same website. Persistent Cross Site Scripting is explained with help of Figure 2.7 taken from [9] in which an attacker exploits stored XSS vulnerability and hijack user's session by submitting his malicious payload.

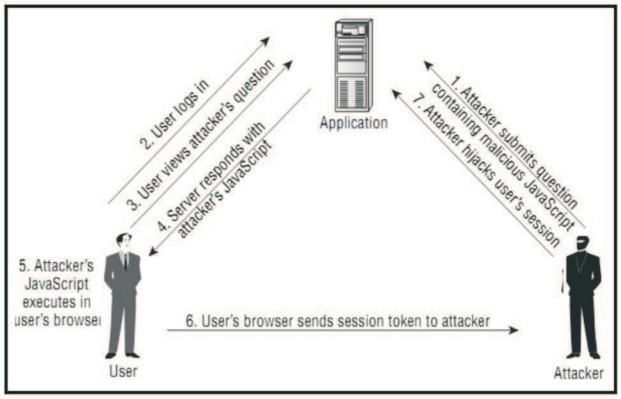

Figure 4: Steps Involved in Stored XSS Attack.

2.2.2. NON-PERSISTENT CROSS SITE SCRIPTING

Non persistent cross site scripting is also called reflected XSS sometimes, another severe form of XSS vulnerability; this vulnerability takes the advantage of weak input validation of the web application. Unlike persistent XSS in which JavaScript is saved in the database, in this type, JavaScript is sent with the request to the vulnerable web application by the victim. The whole scenario is explained with the help of Figure 5 taken from [9].

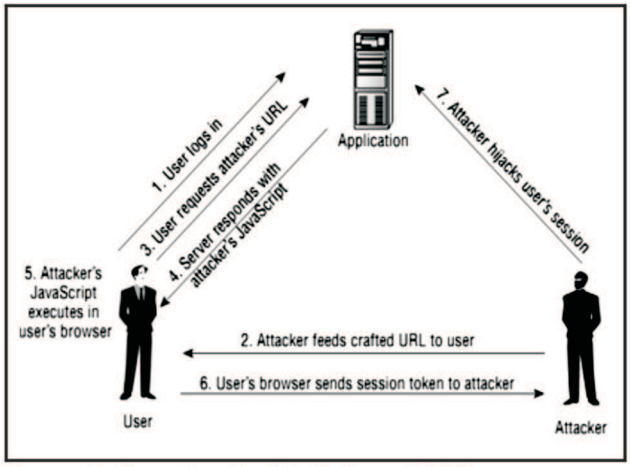

Figure 5: Steps Involved in Reflected XSS.

2.3. PREVENTING CROSS SITE SCRIPTING

The root cause for XSS vulnerability is un-sanitization of user inputs, In order to mitigate Reflected as well as Stored Cross Site Scripting it is necessary to find out all those insertion points in the website which takes user inputs and copy that input into response and sanitize all the inputs. Although there are other solutions suggested by the different authors but defensive coding practice [9], and [17] is more appropriate for defending against XSS.

2.3.1. INPUT VALIDATION

Input validation is the method for accepting all the inputs which the application developer thinks are good. Following are the few points to be noted when validating inputs.

- Data must be validated for permitted length that the data has not exceeded the length that the input field expects.
- Data must be checked for the permitted characters in the input field.
- Last but not the least is that the data must match with the particular regular expression
- The best defense against input validation is the use of Regular Expression

2.3.1. OUTPUT VALIDATION

Output validation is the process of HTML encoding the input returns in response by the application to request made by the end user. HTML encoding sanitizes the inputs for harmful characters by replacing the character with their equivalent objects. HTML encoding ensures that the inputs received will not harm the application logic and will be treated in right manner. The HTML encoding for the few characters which are well known malicious characters are as:

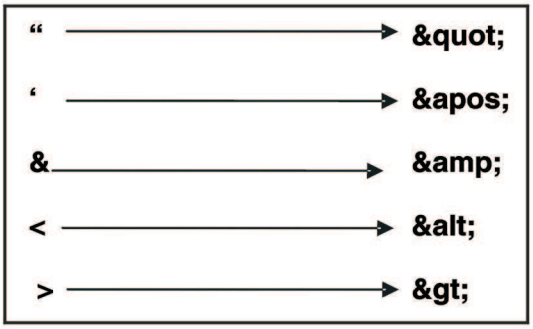

2.4. CROSS SITE REQUEST FORGERY

Cross Site Request Forgery (XSRF) sometimes called one-click attack is a web vulnerability which allows an attacker to send arbitrary request on behalf of user, it takes the advantage of both at server side as well as at client side's browser weak security mechanism. In XSRF attack attacker send JavaScript embedded in the link to the valid user of the website which is vulnerable to XSRF attack. The user is unaware of the attack and the vulnerable website is trusting on the request made by the user browser, as the requests are coming from trusted user's browser therefore server must respond to these requests, Server in this case is unable to identify whether the request is made by the user is a valid request?. Because request is coming from user's browser so there is no conformation about the request made and server blindly believes on the request which is coming from the user's browser. XSRF vulnerability had been exploited by the attackers on some major website such as YouTube, eBay, New York Times, ING Direct, Meta Filter [13]. The explanation of forged request is mentioned in the Figure 5 [13].

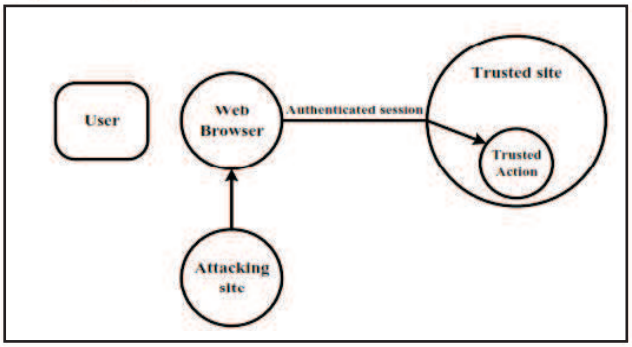

Figure 6: Cross Site Request Forgery attack.

2.5. CROSS SITE REQUEST FORGERY PREVENTION

XSRF Attack only occurs when the server is unable to distinguish whether the request is made by the trusted user which is coming from his browser with the session id issued by the server. In order to stop the exploiting this vulnerability there is a need of special measures which must be taken when making each request to the server. Researchers like [13], [14], [15], and [18] suggested some prevention measures. The prevention measures suggested by [13] are mentioned here. The author has proposed two solutions to this attack:

2.5.1. SERVER SIDE TOOL

The idea behind this tool is that each request made by the user browser must be validated by the server for its authenticity. The author has proposed that a pseudorandom number must be generated by the server which will be stored in the user's cookies as well as in the form's hidden filed. Whenever any request is made by the browser via POST method, the form must contains the pseudorandom number within form's hidden field and also in the cookies which as per Same Origin Policy cannot be altered. In this method whenever an attacker wants to send any request via the browser of trusted user to the vulnerable website, attacker must have to obtain the hidden pseudorandom number that is to be sent to the server and when server receives any request from the trusted user it must validated both filed for pseudorandom number in the form's hidden field as well as in the cookies if both match then request is valid otherwise it is invalid.

2.5.2. CLIENT SIDE TOOL

To protect a user from being the victim of XSRF attack, author has developed a plugin which will protect user from many of the XSRF attacks. The author has implemented this tool as the Firefox extension.

2.6. CROSS SITE TRACING

As discussed earlier that the aim of the attacker in XSS is to hijack user session via getting access to the cookies by any means. In order to stop cookie theft via document.cookie property, Microsoft in 2002 introduced a feature namely HttpOnly. This feature successfully defended the theft of cookies via document.cookie property. The attacker who wants to capture user's cookies in order to hijack user session need to find another way of accessing cookies, as HttpOnly does not allow any JavaScript to get access to the cookies. Cross Site Tracing (XST) is a method which is capable of steeling cookies while HttpOnly feature is in use. White hat security experts after few weeks of introduction of HttpOnly feature, tried to analyze this feature and found a way of accessing a cookies without document.cookie property, the method used by the security expert was the TRACE method which is used for debugging and analysis purpose, by-default enabled on various web servers. Trace method responds to the request made by the user, it replies with all the fields requested by the browser. So if the attacker uses a JavaScript to issue a trace request from user's browser then the request will be responded by the server with the cookies while HttpOnly feature in use. The attack scenario is discussed in detail in this article [16]. The Figure 6 [16] shows the trace method issued for accessing cookies. It is to be noted that, it is not necessary that every TRACE request method will always bring you with the cookies it only works on those web server which supports this feature.

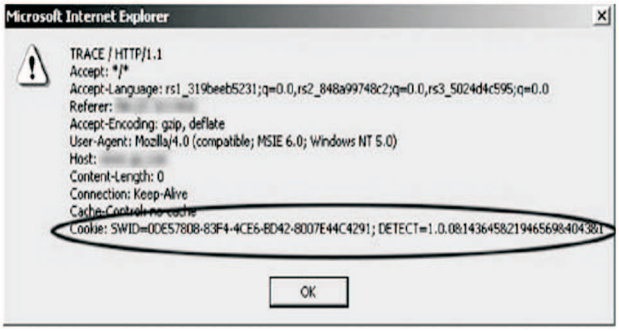

Figure 7: Trace Method for Accessing Cookie.

2.7. XST PREVENTION

There are some general recommendations for preventing the XST attack discussed by the WhiteHat security Experts in this article [16].

- Deactivate the TRACE request method on webservers.
- ActiveX Controls should not be used for scripting.
- Web browsers must be updated so that it can give sufficient protection against domain restriction bypass flaws.
- Users must be educated about disabling the TRACE on web Servers.

3. RESEARCH METHODOLOGY

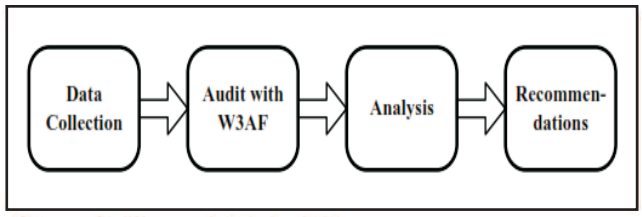

Figure 8: Research Methodology.

3.1. DATA COLLECTION

In order to audit, the most famous websites of Pakistan have been enlisted and divided into three different sectors and equal number of websites from each sector has been chosen so that results may be compared with each other in order to highlight the most vulnerable sector among them

3.2. AUDIT WITH W3AF

In order to conduct penetration test, some penetration scanning tools are required. There are various scanning tools available in market some of them are open source and some of them are business version which can be purchased. w3af tool has been used for scanning. w3af has different types of plugins some of which are explained in later section.

3.2.1. DISCOVERY PLUGIN

Discovery plugin is responsible for finding new URL, forms and other "Injection points" this plugins works like web spider, at input field discovery plugin takes URL and in return discovery plugin gives Injection point.

3.2.2. AUDIT PLUGIN

The Injection points find out by the discovery plugins will be received by the Audit Plugin, and the audit plugin will perform testing so that it can identify the vulnerabilities by sending specially crafted data stored in its database.

3.2.3. GREP PLUGIN

The job of grep plugin is to explore the contents on web page in order to find vulnerabilities for all plugins which needs them.

3.1.4. EXPLOIT PLUGIN

This plugin is used to exploit the vulnerabilities identified in the audit phase.

3.1.5. OUTPUT PLUGIN

The data that is generated by the other plugins is saved in text format, w3af uses its output plugin to facilitate user with this data.

3.2.4. MANGLE PLUGIN

Request and response can be change with mangle plugin.

3.3. ANALYSIS

In this section we present list of audited websites from each sector and highlight the number of vulnerabilities.

RESEARCH FINDINGS

3.3.1. GOVERNMENT SECTOR WEBSITES

In this section most famous websites from government sector has been chosen, the list and audit report of the entire websites from this sector is given in Table 1. The table describes the number and type of the vulnerabilities found in this sector. The results from this sector describe four different types of the vulnerabilities which are SQL Injection, Cross Site Scripting (XSS), Cross Site Request Forgery (XSRF) and Cross Site Tracing (XST). In this sector overall 61 percent of the websites are vulnerable and 39 percent of these websites are safe. The graphical results are shown in Figure 8.

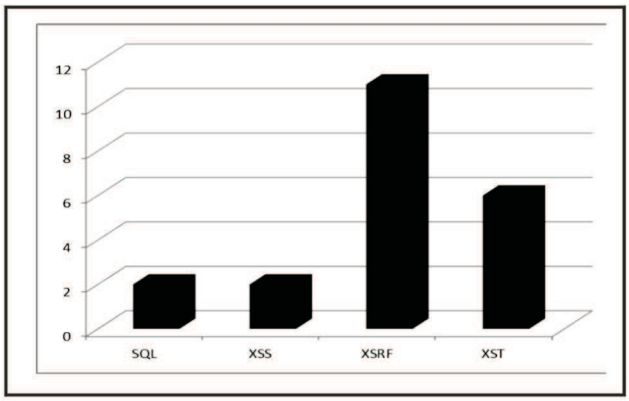

Figure 9: Vulnerability Distribution in Government Sector Websites.

3.3.2. EDUCATION SECTOR WEBSITES

In this section most famous websites from education sector has been chosen, the list and audit report of the entire websites from this sector is mentioned in Table 2. In this sector SQL Injection has not been identified, most of the websites are vulnerable to XSRF attack as well as XST and one website from this category is also

vulnerable to XSS attack. The results are also plotted in the graphical form in Figures 9.

3.2.3. COMMERCIAL SECTOR WEBSITES

In this section the most famous websites from commercial sector has been chosen, the list of vulnerabilities of the entire websites from this sector is given below in Table 3. Commercial Sector websites are mostly vulnerable to XSRF attack as shown in figure 10.

Table 1: Audit List of Govt. Sector Websites.

S.#	Websites	SQL	XSS	XSRF	XST
1.	www.tourism.gov.pk	0	0	0	0
2.	www.fdsindh.gov.pk	0	1	1	0
3.	www.sindh.gov.pk	0	0	0	0
4.	www.finance.gov.pk	0	0	0	0
5.	www.e-government.gov.pk	0	0	0	1
6.	www.cbr.gov.pk	0	0	0	0
7.	www.na.gov.pk	0	0	1	0
8.	www.karachicity.gov.pk	0	0	0	0
9.	www.secp.gov.pk	0	0	1	0
10.	www.pakpost.gov.pk	0	0	0	0
11.	www.pta.gov.pk	0	0	1	0
12.	www.nadra.gov.pk	0	0	4	2
13.	www.moitt.gov.pk	0	0	0	1
14.	www.sngpl.gov.pk	0	0	0	1
15.	www.kse.com.pk	0	0	0	0
16.	www.fbr.gov.pk	0	0	2	0
17.	wwww.nbp.com.pk	0	0	0	0
18.	www.sbp.org.pk	0	0	1	0
19.	www.ptv.com.pk	2	0	0	0
20.	www.ppl.com.pk	0	1	0	1
21.	www.savings.gov.pk	0	0	0	0
	Total	**2**	**2**	**11**	**6**

Table 2: Audit List of Education Sector Websites.

S#	Website	SQL	XSS	XSRF	XST
1.	www.pec.org.pk	0	0	2	0
2.	www.hec.gov.pk	0	0	0	0
3.	www.neduet.edu.pk	0	0	0	1
4.	www.uok.edu.pk	0	0	0	1
5.	www.muet.edu.pk	0	0	0	1
6.	www.usindh.edu.pk	0	0	0	1
7.	www.au.edu.pk	0	0	0	0
8.	www.iqra.edu.pk	0	0	1	0
9.	www.nust.edu.pk	0	0	0	0
10.	www.lumhs.edu.pk	0	0	0	0
11.	www.quest.edu.pk	0	0	0	0
12.	www.giki.edu.pk	0	0	0	1
13.	www.iba-suk.edu.pk	0	0	0	0
14.	www.szabist.edu.pk	0	1	1	0
15.	www.qau.edu.pk	0	0	1	1
16.	www.nu.edu.pk	0	0	0	0
17.	www.ist.edu.pk	0	0	0	0
18.	www.iub.edu.pk	0	0	0	1
19.	www.vu.edu.pk	0	0	0	0
20.	www.hamdard.edu.pk	0	0	0	1
21.	www.nts.org.pk	0	0	0	0
	Total	**0**	**1**	**5**	**8**

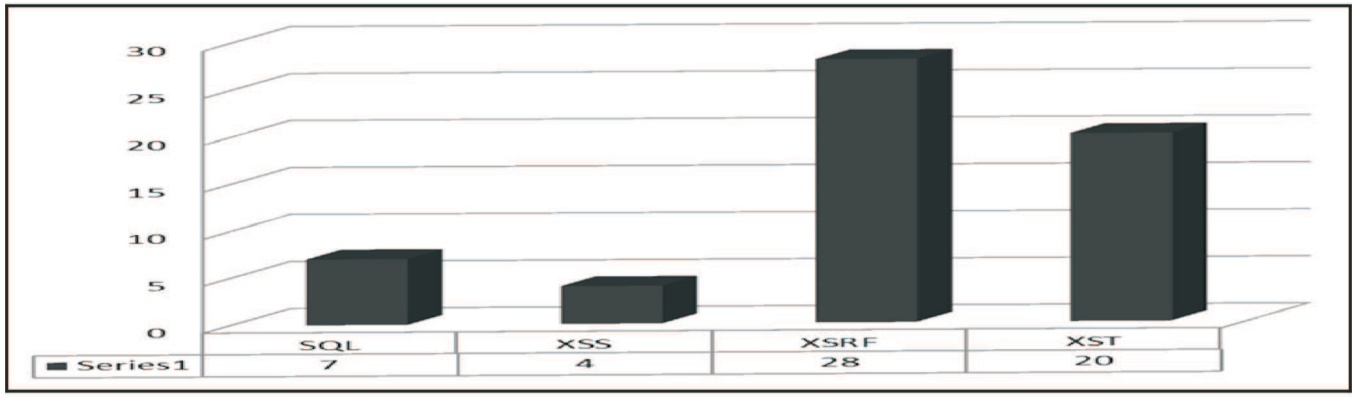

Figure 12: Number of time each vulnerability identified in all 63 websites.

Table 3: Audit list of Commercial Sector Websites.

S.#	Websites	SQL	XSS	XSRF	XST
1.	www.kese.com.pk	0	0	0	0
2.	www.ptcl.com.pk	0	0	1	1
3.	www.pakistanstores.com	1	0	0	0
4.	www.hbl.com	0	0	2	0
5.	www.ubl.com.pk	0	0	1	0
6.	www.mcb.com.pk	0	0	3	1
7.	www.homeshopping.pk	1	0	2	0
8.	www.vmart.pk	0	0	0	1
9.	www.mrlaptop.com.pk	2	0	1	0
10.	www.paperpk.com	1	1	0	0
11.	www.pakistanshopings.com	0	0	0	0
12.	www.galaxy.com.pk	0	0	0	0
13.	www.hamriweb.com	0	0	0	0
14.	www.hbm.com.pk	0	0	0	0
15.	www.honda.com.pk	0	0	0	0
16.	www.cokestudio.com.pk	0	0	0	0
17.	www.nation.com.pk	0	0	1	0
18.	www.zong.com.pk	0	0	0	1
19.	www.bankislami.com.pk	0	0	0	1
20.	www.telenor.com	0	0	1	0
21.	www.inboc.com.pk	0	0	0	1
	Total	**5**	**1**	**12**	**6**

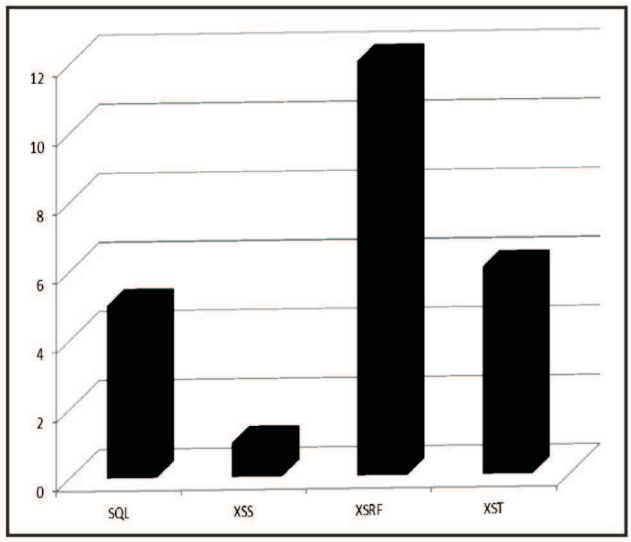

Figure 11: Vulnerabilities in Commercial Sector Websites.

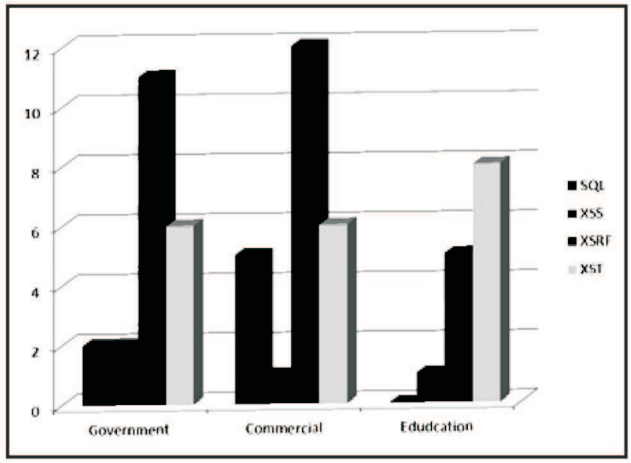

Figure 13: Vulnerability ratios in each sector from websites.

Related Work:

3.3. COMPARISON AMONG THE SECTOR-WISE DISTRIBUTION

In this section the vulnerabilities found in each sector have been compared and the graphs of each sector according to their vulnerabilities are shown in Figures 11, & 12 respectively. Table 4 provides the listing of all the vulnerabilities which were identified in audited websites. Most of the websites are vulnerable to SQL Injection, XSS, XSRF and XST respectively. XSRF and XST are at the top of amongst all mentioned attacks.

Most of the common vulnerabilities, the way attackers exploit them and several related examples are presented in our previous research work in [1]. Here we only highlight the prevention measures related to the SQL injection, XSS, XRF and XST.

Table 4: Comparison of vulnerabilities in each sector.

Vulnerability	Government	Education	Commercial	Total
SQL	2	0	5	7
XSS	2	1	1	4
XSRF	11	5	12	28
XST	6	8	6	20
Total	21	14	24	

Because of SQL Injection's popularity, it is the most discussed by the different authors in [2][3][4] and they have suggested different solutions to the same vulnerability. For example; the parameterized technique has been used in [4] and the input validation method is used in [5], [6] and [7]. The authors in [7] use the regular expression technique that further improves the overall performance. To further enhance the performance of the parameter technique, it has been combined with stored procedure method in [8].

With the help of figures and examples, the authors in [9] detail the prevention method for XSS and explain the way when an attacker exploits stored XSS vulnerability and hijack user's session by submitting his malicious payload. Whereas [9] explains the input and output validation methods related to the defensive coding for the XSS technique.

XSRF vulnerability has been exploited by the attackers on some major website such as YouTube, eBay, New York Times, ING Direct, Meta Filter in [12]. The research work published in [13] and [14] also focuses on the XSRF prevention methods. There are some general recommendations for preventing the XST attack discussed by the WhiteHat security Experts in [15].

4. CONCLUSION & SUGGESTIONS

It has been seen that many websites in Pakistan are being rapidly defaced by the attackers. To find out its causes, the penetration test of some of the most famous websites from different sectors in Pakistan has been conducted in this work. It has been observed that majority of the websites are vulnerable to the security concerns. In order to secure these websites, some solutions have been recommended. Based on these suggestions, a testing website is developed and audited that does not observe any security flaw and hence approve our technique/suggestions. As most of the websites in Pakistan are developed by the newbies who often ignore all the security concern and just focus on the rapid development of these website. It is therefore very important that the web developers must ensure the security of websites by testing websites with suitable scanners at the development time as well on quarterly or (bi) annually so that both the common and new vulnerabilities can be identified and rectified in a timely manner.

REFERENCES

[1] Ali Raza, Asim Imdad Wagan, Zahid Hussain Abro, "Penetration Testing: A survey of web vulnerabilities", QUEST Journal Nawabshah, June 2011, Volume 10, ISSN 1665-8607.

[2] Howard, M., LeBlanc, D, "Writing Secure Code", 2nd Edition, Microsoft Press 2003 publisher, ISBN: 9780735617223.

[3] Halfond, W.G., Viegas, J., Orso, A.: A Classification of SQL-Injection Attacks and Countermeasures. In:

Proc. IEEE Int'l Sym. on Secure Software Engineering (March 2006).

[4] Clarke, J., July 2012, "SQL injection attacks and defense". 2nd Edition, Syngress Publisher, ISBN: 978-1597499637.

[5] Buehrer, G., Weide, B.W., Sivilotti, P.A.G., 2005. "Using parse tree validation to prevent SQL injection attacks", in: Proceedings of the 5th International Workshop on Software Engineering and Middleware. pp. 106–113, ISBN:1-59593-205-4.

[6] Kern, W., 2011. eGovWDF: "Validation-A new approach to input validation in Web based eGovernment applications", Technical Report.

[7] Jan, Goyvaerts,"Regular Expressions: The Complete Tutorial", First Printing: Feb: 2006, ISBN: 1-4116-7760-9.

[8] Preventing SQL Injection in ASP.NET, 2012. URL:http://www.mikesdotnetting.com/Article/113/Preventing-SQL-Injection-in-ASP.NET.[Last accessed: 20-Nov-2012].

[9] Dafydd, Stuttard, Marcus Pinto "The Web Application Hacker's Handbook: Discovering and Exploiting Security Flaws", ISBN-13: 978-0470170779, Publisher Wiley; 1st edition (October 22, 2007).

[10] Williams, J., Wichers, D., 2010. OWASP top 10–2010. "OWASP Foundation", http://www.owasp.org/ [Last accessed: 15-Nov-2012].

[11] CWE - 2011 CWE/SANS "Top 25 Most Dangerous Software Errors" [WWW Document], 2012. URL http://cwe.mitre.org/top25/ [Last accessed 16-Nov-2012].

[12] ZELLER, W. P., AND FELTEN, E. W. Cross-Site Request Forgeries: Exploitation and Prevention. Tech. rep., Princeton University, 2008.

[13] Siddiqui, M., Verma, D., others, 2011. "Cross site request forgery: A common web application weakness", in: Communication Software and Networks (ICCSN), 2011 IEEE 3rd International Conference On. pp. 538–543.

[14] Luyi Xing, Yuqing Zhang, Shenlong Chen, "A client-based and server-enhanced defense mechanism for cross-site request forgery", 13th international conference on Recent advances in intrusion detection, p. 484–485, 2010, ISBN:3-642-15511-6.

[15] GROSSMAN, J. Cross-Site Tracing (XST).http://www.cgisecurity.com/whitehatmirror/WhitePaper screen.pdf, 2003.

[16] How To: Protect From SQL Injection in ASP.NET [WWW Document], 2012. . URL http://msdn.microsoft.com/en-s/library/ff648339.aspx, [Accessed February 27, 2012].

[17] Lwin Khin Shar and Hee Beng Kuan Tan Nanyang Technological University, Singapore, Published by the IEEE Computer Society, 0018-9162/March-12.

[18] Garskof, Robert. "Apparatus and Methods for Preventing Cross-Site Request Forgery." U.S. Patent Application 12/839,884, filed July 20, 2010.

ISSN 1605-8607

RANKING OF PARAMETERS INFLUENCING ON POWER OUTPUT OF PHOTOVOLTAIC SYSTEMS BY SENSITIVITY ANALYSIS

Abdul Qayoom Jakhrani*, Saleem Raza Samo** and Shakeel Ahmed Kamboh***

ABSTRACT

This paper aims to identify the most important and sensitive input variables and to prioritize the parameters based on their influence on the model outputs of a standalone photovoltaic system. Three sensitivity methods, such as sensitivity index, sensitivity coefficient variance and correlation coefficient were applied for the determination of parameter response by one variable at a time method. A total of seven input variables namely slope, solar azimuth angle, hour angle, ground reflectance, amount of total solar radiation, ambient temperature and wind speed were examined with reference to three output parameters. It was revealed that the most important and sensitive input variable was the amount of total solar radiation and the least important variables was solar azimuth angle and the lowest sensitive variable was wind speed. The higher sensitivity variance is displayed by slope followed by hour angle. Insignificant variance is noted in the results of solar azimuth angle and wind speed for all output parameters. It is concluded that the amount of solar radiation, ambient temperature and slope of the system have significant influence over the model results among all examined variables.

Keywords: parameter ranking, sensitivity analysis, sensitivity index, sensitivity coefficient variance, correlation coefficient, photovoltaic system model.

1. INTRODUCTION

Modern systems and processes are complicated in nature. Their physical investigation is expensive or sometimes even impossible. Therefore, the investigators turned to mathematical or computational models to predict or approximate the behavior of systems and processes [1, 2]. The common problem in the models is that, the role of various parameters is not obvious. Generally, important parameters, effects of changing parameters and uncertainties of model results due to uncertainty of model inputs are not known. In many applications, this information is exactly needed. Such knowledge is crucial for the evaluation of model suitability, identification of most influential and sensitive parameters, and for understanding of the systems behavior [3].

The researchers used various terms for describing the influence level of input parameters such as sensitive, important, most influential, major contributor, effective or correlated [4, 5]. The term important was used for those parameters whose uncertainty contributes considerably to the uncertainty in assessment results. The word sensitive referred to those parameters which have a significant influence on output results [6]. However, the main parameter is always sensitive because the parameter changeability will not emerge in the results unless the model is sensitive to the input [7]. A sensitive parameter is not necessarily important because it may have little contribution in the output variability [5]. Different scholars rather used different sensitivity rankings by using different methods according to the nature of analysis and required accuracy.

* Assistant professor, Department of Energy and Environment Engineering, Quaid-e-Awam University of Engineering, Science and Technology (QUEST) Nawabshah

** Professor, Department of Energy and Environment Engineering, Quaid-e-Awam University of Engineering, Science and Technology (QUEST) Nawabshah

*** Lecturer, Department of Mathematics and Statistics, Quaid-e-Awam University of Engineering, Science and Technology (QUEST) Nawabshah

PhD Student, Faculty of Computer Science and Information Technology, Universiti Malaysia Sarawak (UNIMAS), Sarawak, Malaysia

1.1. METHODS OF SENSITIVITY ANALYSIS

Several sensitivity analysis methods could be found in literature from simple to more comprehensive and complicated ones. In brief, these methods includes, one-at-a-time design, differential analysis, factorial design, the derivation of sensitivity and importance indices, subjective analysis, construction of scatter plots, the relative deviation method, relative deviation ratios, correlation coefficients, rank transformation, rank correlation coefficients, partial correlation coefficients, regression techniques, standardized regression techniques, the Smirnov test statistic, the Cramer-von Mises test, Mann-Whitney test, and the squared ranks test [8-12]. Another method for determining parameter sensitivity was given by Hoffman and Gardner [13], which is based on the output % difference by varying one input parameter from its minimum value to its maximum value [14]. Hamby [5] and [14] and Bauer and Hamby [15] conducted a detailed performance of many individual indices relative to a composite index. Their results showed that the model proposed by Hoffman and Gardner [13] performs well for the sensitivity analysis of parameters as compared to ten selected indices. Furthermore, different sensitivity analysis (SA) methods have different characteristics, theories and range of applications. Therefore, the choice of a sensitivity analysis method is generally depends on the sensitivity measure employed, the required precision in the estimates of the sensitivity measure, and the computational cost involved [10, 14].

1.2. SENSITIVITY ANALYSIS OF PHOTOVOLTAIC SYSTEM PARAMETERS

Jakhrani et al [16] conducted sensitivity analysis of model input variables upon output parameters for a standalone photovoltaic system. The input variable includes amount of solar radiation, hour angle, solar azimuth angle, ground reflectance, slope of solar modules, wind speed and ambient temperature. The output parameters were absorbed solar radiation, maximum power output of a PV module and the required area of PV module. El Shatter and Elhagry [17] carried out sensitivity analysis (SA) of unknown parameters such as series resistance (R_s), shunt resistance (R_{sh}), light generated current (I_{ph}), reverse diode saturation current (I_o), and ideality factor (n) with suggested fuzzy input parameter (h) from 0.2 to 0.8 and output parameter (e) around 10%. They found that the PV module parameters were severely affected by temperature variation. Kolhe et al. [18] conducted an economic feasibility of a standalone photovoltaic (SAPV) system and a diesel generator. The fuel consumption rate was compared versus diesel generator rated power capacity at different load factors. They also analyzed PV/diesel life cycle cost ratio against cost of the photovoltaic (PV) array and diesel with energy demand. Ito et al. [19] carried out a sensitivity analysis of a very large scale PV system in deserts. They compared the PV module efficiency with generation cost, energy payback time and CO_2 emissions. Loutzenhiser et al. [20] used Monte Carlo and fitted effects for N-way factorial for uncertainty analysis of total solar radiation on a south-west facade building integrated PV system. Cameron et al. [21] analyzed power outputs of different PV models with different PV module technologies at daily and monthly average yearly basis.

Emery [22] evaluated uncertainties of measured PV power output with rated PV power output, and measured current and voltage with junction temperature and solar irradiance. A monthly mean solar radiation with total and beam radiation, PV cell temperature with ambient temperature and energy output for fixed, optimum and tracking PV systems was evaluated by Gang and Ming [23]. Ren et al. [24] conducted sensitivity analysis of levelized cost of energy with capital cost, efficiency, interest rate and electrical sale price. Talavera et al. [25] carried out SA on internal rate of return (IRR) of a grid connected PV system with three scenarios on the parameters of annual yield of PV system, PV module unit price, initial investment and interest rate. The sensitivity of R_s to R_{sh}, R_{sh} to R_s and of current, voltage and power of a single diode PV cell model was conducted by Zhu et al. [26]. Kaabeche et al. [27] carried out a techno-economical valuation of a PV system on hourly solar radiation, wind speed and ambient temperature versus time. The authors compared number of PV modules with storage capacity of different autonomy days and total annualized cost with different deficiencies of power supply probabilities and net present cost with various discount rates, capital cost and project life. The uncertainty analysis of a double diode model was

conducted by Adamo et al. [28]. They compared the amount of solar irradiance versus temperature, mean relative estimation error on R_s and R_{sh}, and standard deviation on R_s and R_{sh}.

The sensitivity analysis on levelized cost of electricity versus interest rate with the inputs of initial installation cost of PV system, energy output and degradation rate was carried out by Branker et al. [29]. They compared discount rate versus initial installation cost of PV system with the inputs of lifetime loan term, energy output, degradation rate and zero interest loans. They also evaluated lifetime of PV system versus initial installation cost of PV system with the inputs of discount rate, energy output, degradation rate, and zero interest loan. Dufo-Lopez et al. [30] applied Strength Pareto Evolutionary Algorithm to the multi-objective optimization of standalone PV-wind-diesel system with battery storage. They conducted SA on parameters like inflation of diesel cost, acquisition cost and emissions of PV panels. Andrews et al. [31] presented a methodology for fine resolution modeling of a PV system using PV module short circuit current (I_{sc}) at 5-min time-scales. They identified the pertinent error mechanisms by filtering the data with regressive analysis. Mbaka et al. [32] carried out an economic evaluation among three different power producing systems such as PV hybrid system, standalone PV system and standalone diesel generator system using net present value cost. SA was conducted on diesel prices and the unit cost of PV modules.

It is revealed from the literature review that the most of the sensitivity analysis methods are used for the analysis of biological, environmental, water quality parameters and chemical kinetics. These are rather new in the analysis of PV system parameters. No complete sensitivity analysis of PV system input variables as a function of output parameters has been found in the literature. Most of the sensitivity analysis was conducted on the cost analysis of the systems and a few on the parameters of equivalent electrical circuit characteristics of PV modules. Equivalent electrical circuit (I-V characteristic curve) parameters are implicit in nature and their performance itself depends upon the values of other input variables such as slope, solar azimuth angle, hour angle, ground reflectance, monthly average daily total solar radiation, ambient temperature and wind speed. The influence of these input variables is not studied by the former researchers. Therefore, the assessment of their effect is crucial for the evaluation of model suitability, identification of the most influential and sensitive parameters for the system design and performance prediction. Thus a sensitivity analysis is carried out to understand the system behavior and to investigate the response of PV system models with respect to the variation in input variables. In this study, sensitivity index has been used, which is computationally efficient technique that allows rapid preliminary examination of the model. It also provides the slope of the calculated model output in parameter space at a given set of values. Furthermore, sensitivity coefficient variance and correlation coefficients have been determined for the analysis of parameters variation due to the changing of input variables.

2. METHODOLOGY

Kuching with latitude (ϕ) of 1.48^{o} N was selected for this analysis due to availability of recorded solar radiation data of the area. Worst (lowest radiation) month method was used for this study. Since, January is the lowest solar radiation month in Kuching. The long term average value of a single day i.e. 17^{th} day of January $(n = 17)$, which characterizes similar monthly average values were used for this analysis as adopted by Jakhrani et al. [33]. Five input variables namely slope (β), solar azimuth angle (γ), hour angle (ω), ground reflectance or albedo (ρ_g) and monthly average daily total solar radiation $(\overline{H}_T)$ with three constants such as solar constant $(G_{sc} = 1367\ W/m^2)$ were used for calculation of absorbed solar radiation (S_T). The absorbed solar radiation (S_T) with two other variables namely ambient temperature (T_a) and wind speed (V_w) were used as input for the estimation and assessment of PV module maximum power output (P_{max}) and optimum PV array area (A_{opt}) as shown in Figure 1.

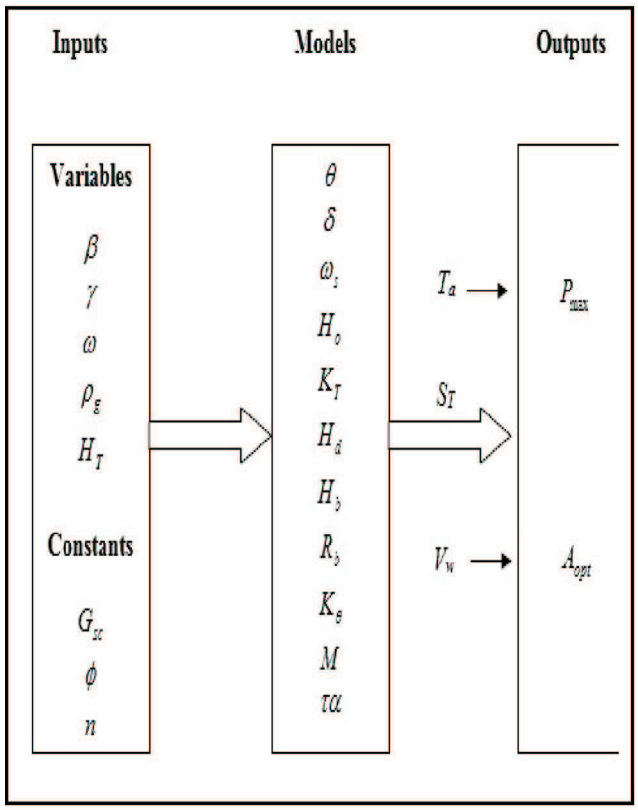

Figure 1. Model for sensitivity analysis of photovoltaic system parameters

Sensitivity analysis results were validated using different models for estimation of power output with various input values of solar radiation ambient temperatures. The models used for this study were Evans [34], Borowy BS, Salameh [35], Hove [36], Jie et al. [37] and Jakhrani et al. [38]. Sensitivity analysis of model parameters was carried out by means of differential analysis method. In first step of analysis, the base values, ranges and distributions were selected for each input variable. Secondly, a Taylor series approximation to the model output was developed close to the base values of the model inputs. The first order Taylor series was preferred. Thirdly, the variance propagation techniques were used for the estimation of the uncertainty in model output in terms of its projected values and variance, because these values changes according to the order of approximation. Finally, the first order Taylor series was used to estimate the magnitude of each input parameter [39]. Three sensitivity analysis methods such as sensitivity variance, sensitivity index and correlation coefficients have been adopted for the evaluation of three output parameters such as absorbed solar radiation (S_T), PV module maximum power output (P_{max}) and optimum PV array area (A_{opt}). The algorithm proposed by Hoffman and Gardner [13] is used for the determination of sensitivity index of parameters. It is given as:

$$SI = \frac{y_{max} - y_{min}}{y_{max}} \quad (1)$$

where SI is the sensitivity index, y_{min} and y_{max} represent the minimum and maximum output values, respectively. The changes in the results of output parameters with respect to changes in input variables are calculated by means of parameter variance (V) [6].

$$V = \frac{1}{n}\sum_{i=1}^{n} (\tilde{S}_i - \bar{\tilde{S}})^2 \quad (2)$$

where $\tilde{S}_i$ is the local normalized coefficient and represents a linear estimate of the percentage change in the variable y caused by a one percent change in the parameter x. $\bar{\tilde{s}}$ is the arithmetic mean of $\tilde{S}_i$ and n is the number of data points in $\tilde{S}_i$. Moreover, the strength and significance of the linear relationship between the input variable x and output variable y in the regression equation is measured by correlation coefficient (r). Its values are always between -1 and 1. Therefore, the dependence of output parameter y on a single input variable x is determined by Pearson correlation coefficient and is defined as [2, 14]:

$$r_{xy} = \frac{\sum_{i=1}^{n}(y_i - \bar{y})(x_i - \bar{x})}{\sqrt{\sum_{i=1}^{n}(y_i - \bar{y})^2 \sum_{i=1}^{n}(x_i - \bar{x})^2}} \quad (3)$$

3. RESULTS AND DISCUSSIONS

The values of input parameters were varied around the base values of parameters. The slope (β) was changed with an interval of five degrees from 0° to 90°. The comparative values of sensitivity coefficient variance, sensitivity index and correlation coefficient of output parameters at various slopes are shown in Figure 2.

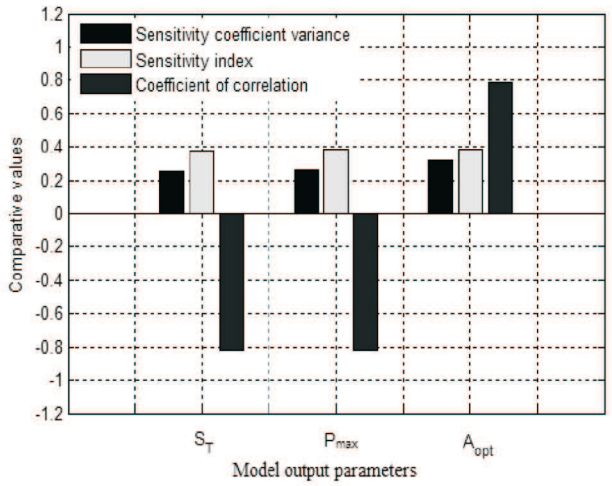

Figure 2. Values of output parameters by different sensitivity methods at various slopes (β)

The obtained sensitivity coefficient variance was 0.2518, 0.2658 and 0.3216, the sensitivity index was 0.3794, 0.3847 and 0.3847, and the correlation coefficient was -0.8219, -0.8211 and 0.7891 for output values of S_T, $P_{\max}$ and A_{opt} respectively. The higher sensitivity variance and sensitivity index was observed in optimum PV array area (A_{opt}) as compared to absorbed solar radiation (S_T) and maximum PV module power output $(P_{\max})$. Negative correlation coefficient was noted in both absorbed solar radiation and maximum PV power output, whereas, the positive correlation was observed in optimum PV array area.

The input values of the solar azimuth angle (γ) were varied with an interval of 10° from -90° to +90°. The *- comparative results of sensitivity coefficient variance, sensitivity index and correlation coefficient of output parameters at various solar azimuth angles are shown in Figure 3. It is discovered from the analysis that variance and correlation coefficient in the results of solar azimuth angle was found to be zero and one respectively. However, the sensitivity index of all output parameters were approximately 0.38.

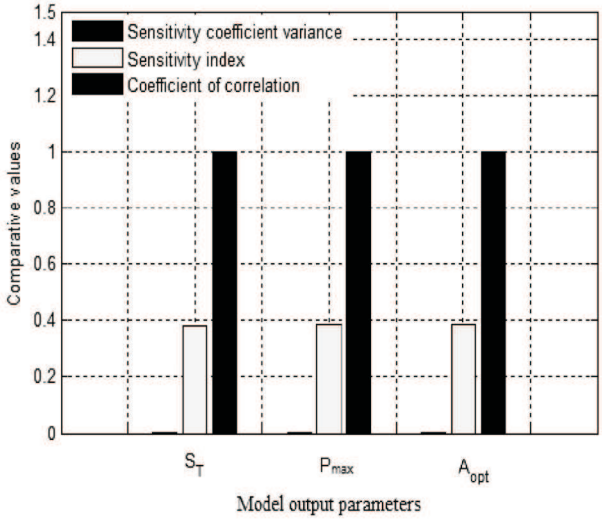

Figure 3. Values of output parameters by different sensitivity methods at various solar azimuth angles (γ)

The input values of the hour angle (ω) were varied with an interval of 15° from -75° to +75 °. The comparative values of sensitivity coefficient variance, sensitivity index and correlation coefficient of output parameters at various hour angles are shown in Figure 4. The variance of S_T was almost zero, whereas, the variance in the results of $P_{\max}$ and A_{opt} were 0.11 and 0.09 respectively. The sensitivity index and correlation coefficient of all three output variables were 0.17 and 1.0 respectively.

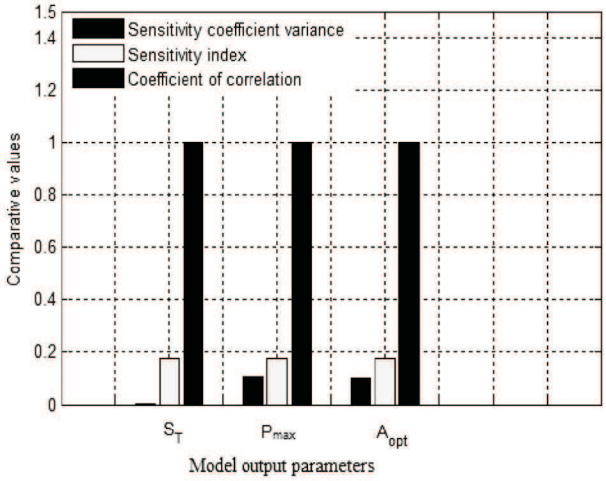

Figure 4. Values of output parameters by different sensitivity methods at various hour angles (ω)

The input values of ground reflectance (ρ_g) were varied by an interval of 0.1 from 0.0 to 0.7. The relative values of sensitivity coefficient variance, sensitivity index and correlation coefficient of output parameters at various ground reflectance (ρ_g) inputs are shown in Figure 5. The variance in the results of S_T, P_{max} and A_{opt} were 0.0064, 0.0061 and 0.0057, and sensitivity index were 0.251, 0.2492 and 0.2492 respectively. The correlation coefficient of all three output parameters with respect to input variables was unity.

The input values of monthly mean daily total solar radiation on horizontal surface ($\overline{H}$) were changed with an interval of 1.0MJ/m^2 from 5.0 to 25.0MJ/m^2. The results of sensitivity coefficient variance, sensitivity index and correlation coefficient of output parameters at monthly mean daily total solar radiation are shown in Figure 6. The variance in the results of S_T, P_{max} and A_{opt} were 0.0, 0.0035 and 0.0007, and sensitivity index were 0.8071, 0.8069 and 0.8069 respectively. The correlation coefficient were found to be unity, in all three output variables such as S_T, P_{max} and A_{opt}.

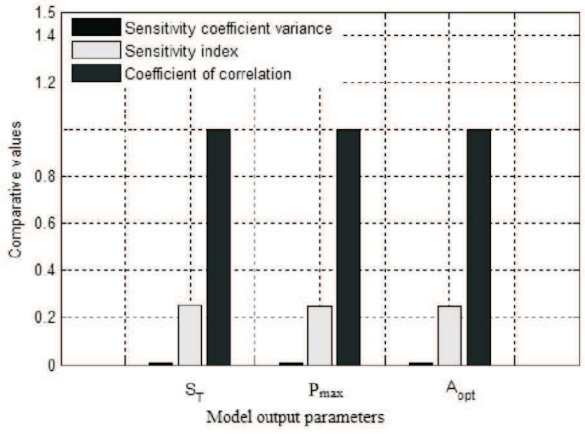

Figure 5. Values of output parameters by different sensitivity methods at various input values of ground reflectance (ρ_g)

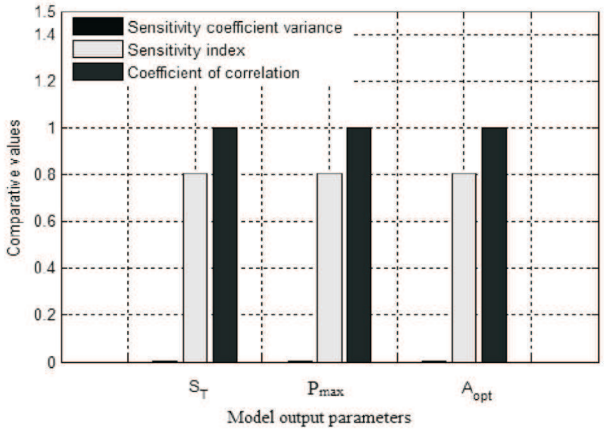

Figure 6. Values of output parameters by different sensitivity methods at various levels of total solar radiation ($\overline{H}$)

The input values of ambient temperature (T_a) were changed with an interval of 5°C from 15°C to 50°C. The comparative values of sensitivity coefficient variance, sensitivity index and correlation coefficient of output parameters namely P_{max} and A_{opt} at various ambient temperature (T_a) levels are shown in **Figure 7**. The variance in P_{max} and A_{opt} were found to be 0.0068 and 0.0074. The sensitivity index and the correlation coefficient for both output parameters (P_{max} and A_{opt}) were 0.21 and 1.0 respectively.

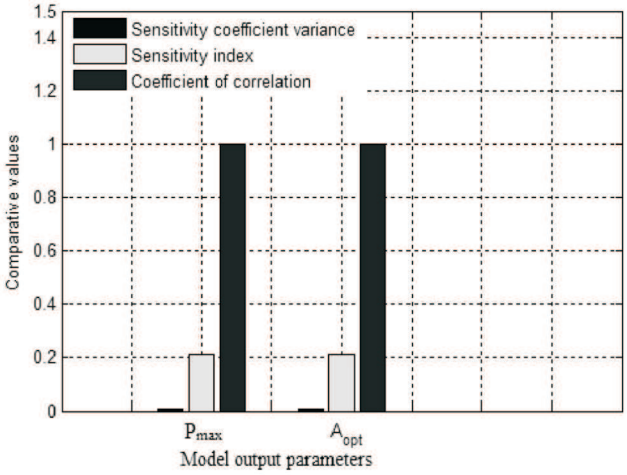

Figure 7. Values of output parameters by different sensitivity methods at various levels of ambient temperature (T_a)

The input values of wind speed (V_w) were changed with an interval of 1m/s from zero to 10m/s. The comparative values of sensitivity coefficient variance, sensitivity index and correlation coefficient of output parameters such as $P_{\max}$ and A_{opt} at various wind speed levels are shown in Figure 8. The variance, the sensitivity index and the correlation coefficient for both output parameters were found to be 0.0001, 0.033 and 1.0 respectively.

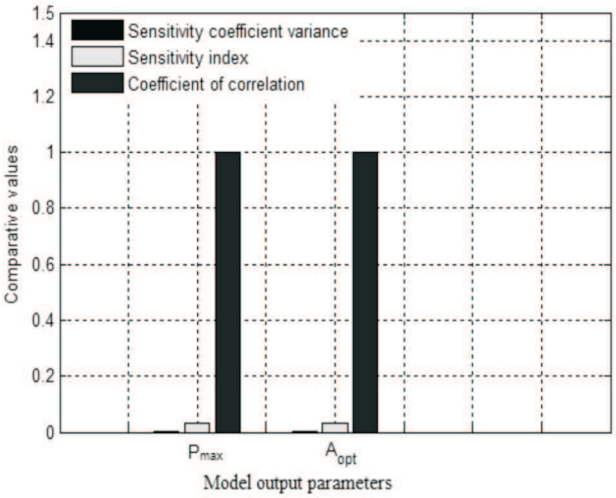

Figure 8. Values of output parameters by different sensitivity methods at various wind speed (V_w)

The overall sensitivity coefficient of variance of output parameters such as S_T, $P_{\max}$ and A_{opt} with respect to input variables namely slope (β), solar azimuth angle (γ), hour angle (ω), ground reflectance (ρ_g), total solar radiation $(\overline{H})$, ambient temperature (T_a) and wind speed (V_w) are given in **Figure 9**. The higher sensitivity variance is displayed by slope (β) with more than 0.25 for all output parameters followed by hour angle (ω) with the variance of 0.1. Less variance is observed for the input variable of ground reflectance (ρ_g), total solar radiation $(\overline{H})$ and ambient temperature (T_a). Negligible variance is noted in the results of solar azimuth angle (γ) and wind speed (V_w) for all output parameters.

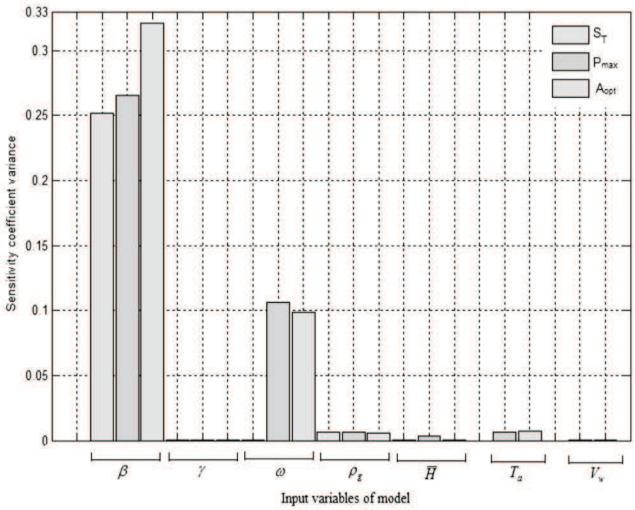

Figure 9. Sensitivity coefficient variance of output parameters versus different input variables

The sensitivity index of all output parameters with respect to input variables are illustrated in **Figure 10**. The highest sensitivity index is shown by total solar radiation $(\overline{H})$ with the sensitivity index of 0.8 in all output parameters. The second and third most sensitive variables were found to be slope (β) and solar azimuth angle (γ), both with the sensitivity index of approximately 0.4. The sensitivity index of ground reflectance (ρ_g) was approximately 0.25, the ambient temperature (T_a) with 0.20 and the hour angle (ω) with 0.18. The lowest sensitive variable was found to be wind speed (V_w) with the index less than 0.1.

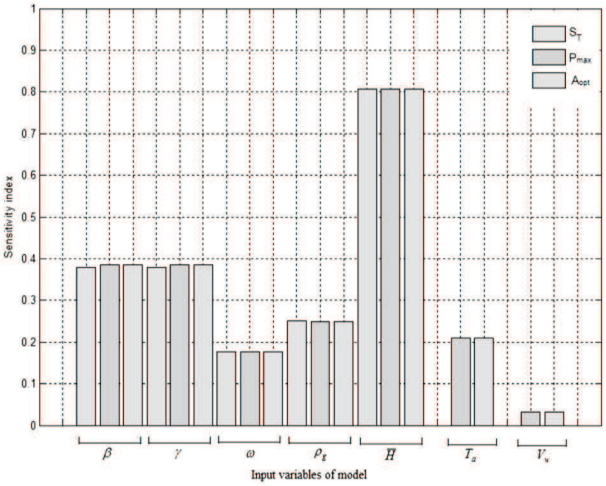

Figure 10. Sensitivity indices of output parameters versus different input variables

The results of correlation coefficient of input variables and output parameters are given in Figure 11. It is found that almost all output parameters displayed higher correlation with input variables except the slope (β). The negative correlation is observed by the input variable of slope (β) for the amount of absorbed solar radiation (S_T) and maximum PV module power output $(P_{\max})$ and positive correlation with optimum PV array area (A_{opt}) with the index of 0.8.

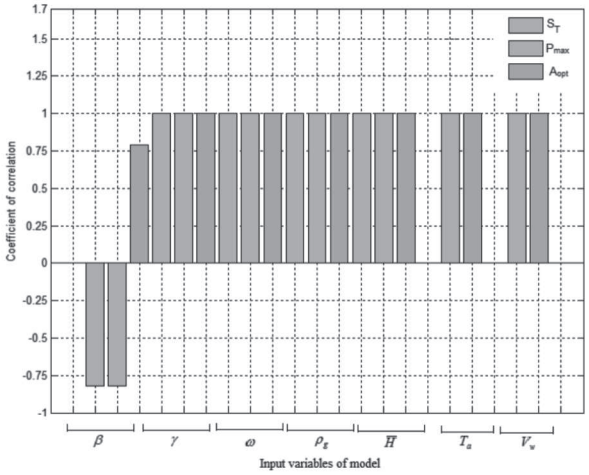

Figure 11. Correlation coefficient of output parameters versus different input variables

The comparison of PV module power out estimations with respect to solar radiation and ambient temperature by various models are given in Figures 12 and 13. It was observed that all model results are mutually consistent and the tendency of model variations was same. Therefore, it was deduced that sensitivity of parameters will be identical due to similar mode of model estimated values.

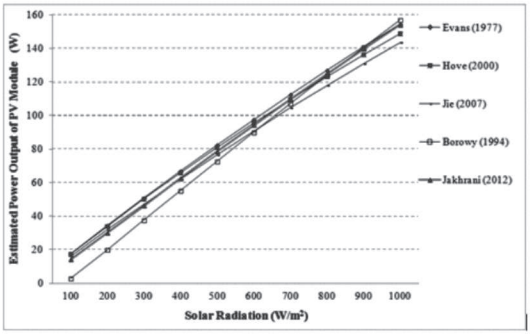

Figure 12. Comparative results of PV module power output versus monthly mean daily solar radiation at constant ambient temperature

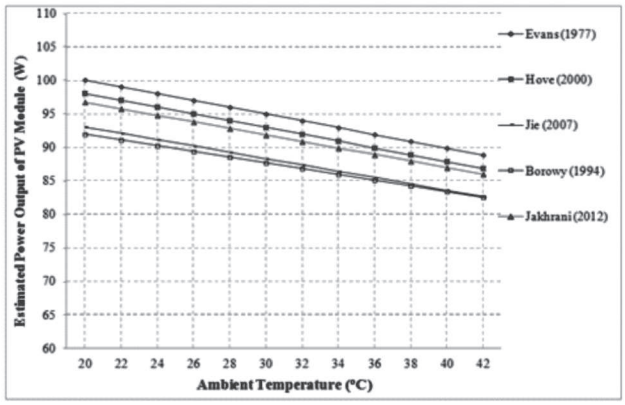

Figure 13. Comparative results of PV module power output versus ambient temperature at a constant solar radiation

It is revealed from the sensitivity analysis of input variables and output parameters that the most important input variable was the amount of total solar radiation $(\overline{H})$ because of its high contribution in changing the amount of absorbed solar radiation (S_T) level. The changes took place by amount of total solar radiation $(\overline{H})$ in the output variables were approximately 2.5 times when its amount was varied around its typical ranges followed by slope (β) with 61%, ground reflectance (ρ_g) 33%, ambient temperature (T_a) 23% and hour angle (ω) 20%. The less important variables were found to be wind speed (V_w) 4% and solar azimuth angle (γ) less than one percent as per one-at-a-time (OAT) method. The highest sensitive input variable was found to be total solar radiation $(\overline{H})$ with the index of 0.8, followed by slope (β), solar azimuth angle (γ), ground reflectance or albedo (ρ_g), the ambient temperature (T_a) and the hour angle (ω). The lowest sensitive variable was found to be wind speed (V_w) with the index less than 0.1.

4. CONCLUSIONS

The results of sensitivity analysis parameters revealed that the most important input variable was the amount of total solar radiation $(\overline{H})$ because of its high contribution in modifying the amount of absorbed solar radiation (S_T) level, PV module power output $(P_{\max})$ and

optimum PV array area (A_{opt}). The changes contributed by amount of total solar radiation ($\overline{H}$) in the output variables are approximately 2.5 times when its amount was varied around its typical ranges. The second most important parameters were slope (β) with 61% and the less important important variable was found to be solar azimuth angle (γ) with less than one percent influence over the output results as per one-at-a-time (OAT) method. Similarly, the highest sensitive input variable was found to be total solar radiation ($\overline{H}$) with the index of 0.8. The second sensitive variable was slope (β) with 0.38 and the lowest sensitive variable was found to be wind speed (V_w) with the index less than 0.1.

The higher sensitivity variance is displayed by slope (β) with more than 0.25 for all output parameters followed by hour angle (ω) with the variance of 0.1. The negligible variance is noted in the results of solar azimuth angle (γ) and wind speed (V_w) for all output parameters.

All output parameters displayed higher correlation with input variables except the slope (β). It displayed negative correlation for the amount of absorbed solar radiation (S_T) and maximum PV module power output (P_{max}) and positive correlation with optimum PV array area (A_{opt}) with the index of 0.8.

The following conclusions were drawn from this study:

- The most important and sensitive variable was found to be solar radiation and least important variable was solar azimuth angle and the least sensitive variable was wind speed.
- The higher coefficient variance was displayed by slope followed by hour angle and insignificant variance is displayed by solar azimuth angle and wind speed.
- Almost all output parameters displayed higher correlation with input variables except slope of PV modules.
- Three input variables namely the amount of solar radiation, ambient temperature and slope have governing influence over the model results.

REFERENCES

[1] Fellin W, Lessmann H, Oberguggenberger M, Vieider R. Analyzing uncertainty in civil engineering. 1st ed., Springer, 2004. p. 1-251.

[2] Saltelli A, Ratto M, Tarantola S, Campolongo F. Sensitivity analysis practices: Strategies for model-based inference. Reliability Engineering and System Safety. 2006; 91: 1109-1125.

[3] Isukapalli SS, Georgopoulos PG. Computational methods for sensitivity and uncertainty analysis for environmental and biological models. National Exposure Research Laboratory, USEPA/600/R-01-068, 2001. p. 1-145.

[4] Iman RL, Helton JC. An investigation of uncertainty and sensitivity analysis techniques for computer models. Risk Analysis. 1988; 8: 71-90.

[5] Hamby D. A review of techniques for parameter sensitivity analysis of environmental models. Environmental Monitoring and Assessment. 1994; 32: 135-154.

[6] Saltelli A, Annoni P, Azzini I, Campolongo F, Ratto M, Tarantola S. Variance based sensitivity analysis of model output: Design and estimator for the total sensitivity index. Computer Physics Communications. 2010; 181: 259-270.

[7] Cacuci DG, Ionescu-Bujor M, Navon IM. Sensitivity and uncertainty analysis; V-II: Applications to large-scale systems. 1st ed., CRC Press, 2005. p. 1-368.

[8] Cukier R, Levine H, Shuler K. Nonlinear sensitivity analysis of multiparameter model systems. Journal of Computer Physics. 1978; 26: 1-42.

[9] Iman RL, Hora SC. A robust measure of uncertainty importance for use in fault tree system analysis. Risk Analysis. 1990; 10: 401-406.

[10] Bell WR, Otto MC. Bayesian assessment of uncertainty in seasonal adjustment with sampling error present. Research Report, U.S Bureau of the Census, 1992. p. 26-38.

[11] Bekele EG, Nicklow JW. Multi-objective automatic calibration of SWAT using NSGA-II. Journal of Hydrology. 2007; 341: 165-176.

[12] Zakayo S. Multi-objective calibration of SWAT model for pesticide simulations. Interantional SWAT Conference, SWAT, Boulder, Colorado, August 5-7, 2009. p. 1-16.

[13] Hoffman FO, Gardner RH. Evaluation of uncertainties in environmental radiological assessment models. Radiological assessment: A textbook on environmental dose assessment. US Nuclear Regulatory Commission, Washington, DC. NUREG/CR-3332, ORNL-5968, 1983. p. 1-882.

[14] Hamby D. A comparison of sensitivity analysis techniques. Health Physics. 1995; 68: 195-204.

[15] Bauer L, Hamby D. Relative sensitivities of existing and novel model parameters in atmospheric tritium dose estimates. Radiation Protection Dosimetry. 1991; 37: 253-260.

[16] Jakhrani AQ, Othman AK, Rigit ARH, Samo SR, Kamboh SA. Sensitivity analysis of a standalone photovoltaic system model parameters. Journal of Applied Sciences, 2013: 13 (2): 220-231.

[17] El Shatter T, Elhagry M. Sensitivity analysis of the photovoltaic model parameters, 42nd Midwest Symposium on Circuits and Systems. New Mexico State University, Las Cruces, NM, 8-11 August, 1999. p. 914-917.

[18] Kolhe M, Kolhe S, Joshi J. Economic viability of stand-alone solar photovoltaic system in comparison with diesel-powered system for India. Energy Economics. 2002; 24: 155-165.

[19] Ito M, Kato K, Komoto K, Kichimi T, Kurokawa K. A Sensitivity analysis of very large-scale photovoltaic power generation (VLS-PV) systems in deserts. IEEE 4th World Conference on Photovoltaic Energy Conversion, Waikoloa, Hawaii, USA, 8-12 May, 2006. p. 2387-2390.

[20] Loutzenhiser P, Manz H, Felsmann C, Strachan P, Frank T, Maxwell G. Empirical validation of models to compute solar irradiance on inclined surfaces for building energy simulation. Solar Energy. 2007; 8: 254-267.

[21] Cameron CP, Boyson WE, Riley DM. Comparison of PV system performance-model predictions with measured PV system performance. Proceedings of 33rd IEEE PVSC, San Diego, CA, 2008. p. 1-6.

[22] Emery K. Uncertainty analysis of certified photovoltaic measurements at the National Renewable Energy Laboratory. NREL, USA, 2009. p. 1-59.

[23] Gang Y, Ming C. Methodology for precisely estimating the generation of standalone photovoltaic system. ESIAT, Wuhan, China, 4-5 July, 2009. p. 48-51.

[24] Ren H, Gao W, Ruan Y. Economic optimization and sensitivity analysis of photovoltaic system in residential buildings. Renewable Energy. 2009; 34: 883-889.

[25] Talavera D, Nofuentes G, Aguilera J. The internal rate of return of photovoltaic grid-connected systems: A comprehensive sensitivity analysis. Renewable Energy. 2010; 35: 101-111.

[26] Zhu XG, Fu ZH, Long XM. Sensitivity analysis and more accurate solution of photovoltaic solar cell parameters. Solar Energy. 2011; 85: 393-403.

[27] Kaabeche A, Belhamel M, Ibtiouen L. Techno-economic valuation and optimization of integrated photovoltaic/wind energy conversion system. Solar Energy. 2011; 85: 2407-2420.

[28] Adamo F, Attivissimo F, Di Nisio A, Spadavecchia M. Analysis of the uncertainty of the double-diode model of a photovoltaic panel. IEEE I2MTC, Hangzhou, China, May 10-12, 2011.

[29] Branker K, Pathak M. Pearce J. A review of solar photovoltaic levelized cost of electricity. Renewable and Sustainable Energy Reviews. 2011; 15: 4470-4482.

[30] Dufo-Lopez R, Bernal-Agustin JL, Yusta-Loyo JM, Dominguez-Navarro JA, Ramirez-Rosado IJ, Lujano

J. Multi-objective optimization minimizing cost and life cycle emissions of stand-alone PV-wind-diesel systems with batteries storage. Applied Energy. 2011; 88: 4033-4041.

[31] Andrews RW, Pollard A, Pearce JM. Improved parametric empirical determination of module short circuit current for modelling and optimization of solar photovoltaic systems. Solar Energy. In press, 2012.

[32] Mbaka NE, Mucho NJ, Godpromesse K. Economic evaluation of small-scale photovoltaic hybrid systems for mini-grid applications in far north Cameroon. Renewable Energy. 2010; 35: 2391-2398.

[33] Jakhrani AQ, Samo SR, Rigit ARH, Kamboh SA. Selection of models for calculation of incident solar radiation on tilted surfaces. World Applied Sciences Journal, 2013; 22 (9): 1334-1341.

[34] Evans DL, Florschuetz LW. Cost studies on terrestrial photovoltaic power systems with sunlight concentration. Solar Energy, 1977; 19: 255–262.

[35] Borowy BS, Salameh ZM. Optimum photovoltaic array size for a hybrid wind/PV system. IEEE Transactions on Energy Conversion, 1994; 9: 482–888.

[36] Hove T. A method for predicting long-term average performance of photovoltaic systems. Renewable Energy, 2000; 21: 207–229.

[37] Jie J, Hua Y, Wei H, Gang P, Jianping L, Bin J. Modelling of a novel Trombe wall with PV cells. Building and Environment, 2007; 42:1544–1552.

[38] Jakhrani AQ, Othman AK, Rigit ARH, Baini R, Samo SR, Ling LP. Investigation of solar photovoltaic module power output by various models, NED University Journal of Research, Thematic Issue on Energy, 2012; 25-34.

[39] Helton JC, Davis FJ, Johnson JA. A comparison of uncertainty and sensitivity analysis results obtained with random and Latin hypercube sampling. Reliability Engineering and System Safety. 2005; 89: 305-330.

ISSN 1605-8607

REAL-TIME DRIVER'S VIGILANCE DETECTION SYSTEM

Umair Ali Khan[*], Syed Raheel Hassan[**], Intesab Hussain Sadhayo[***], Zahid Hussain Abro[****]

ABSTRACT

The number of road accidents caused by non-vigilant drivers is increasing rapidly all over the world. Therefore, driver's vigilance detection is an important area of research in intelligent transportation systems. This paper presents an image processing based approach using minimum hardware to detect a driver's fatigue and generate an alarm if the driver is inattentive to driving. The system works in separate modules on each video frame from a smart, low-power, Near Infra-Red (NIR) camera installed at the vehicle's dash board. Our proposed system is based on two trained Haar classifiers to detect driver's face and eyes and then tracking the iris with the method of template matching. Our algorithm updates statistics of the iris's tracking and the direction of gaze in successive video frames. An alarm is generated if the frequency of iris detection in a specific time period goes below a certain threshold or the driver does not concentrate straight to the road. The search area of every module is restricted to a particular region of interest (user-selectable) which increases the detection speed. Fatigue detection through iris tracking by template matching provides a fast means of detecting driver's fatigue. Another module, running in parallel with the face, eyes and iris detection modules tracks the head of the driver. In the situations where the driver is wearing sun glasses, eyes cannot be detected and hence iris cannot be tracked. In this case, head tracking helps to analyze driver's fatigue. We tested our algorithm in the scenarios very close to the real cases (different lighting conditions, subjects, etc). The results presented in this paper show that our algorithm is able to maintain an adequate level of detection accuracy and its minimum architecture makes it best suited for implementation in real scenarios.

1. INTRODUCTION

The lacks of vigilance from drivers pose an imminent threat to road's safety and causes significant number of accidents. Almost 10-20% of the road accidents all over the world result from driver's fatigue [1]. While in the heavy vehicles (e.g., trucks), driver's lack of vigilance causes 60% of the fatal accidents [2]. Moreover, the accidents caused by driver's declined level of attention are far worse than those caused by other factors because the fatigued drivers usually do not take any preventive actions before an accident. Therefore, many countries have invested heavily in building intelligent transportation systems to provide secure transportation and researchers are paying more attention to the driving safety problem to decrease road accidents [26]. Developing systems for detecting drivers' vigilance level and thereby warning them to become attentive are gaining interest among the scientific communities related to intelligent transportation systems. However, an effective solution for this problem should be cost-effective, portable, small-sized, easily implementable, appealing to the end-users, and motivational for the traffic authorities in the enforcement perspective [27]. Such a system should be able to work autonomously in different environmental conditions. Additionally, it must not pose any serious threat to the driver's health.

Among various other techniques, image processing is considered to be more viable and user-friendly approach for determining driver's vigilance level than other approaches such as those based on Electro Encephalon Graph (EEG) which are considered to be intrusive [2]. The most important feature of an image processing based system is that it does not pose any significant challenge in terms of large hardware design, change in road's or vehicle's infrastructure, or a special training to the end-users. Images contain a lot of details which can be manipulated to obtain the required information about a scene. Apart from that, the image processing based

[*] Institute of Networked and Embedded Systems, Alpen-Adria Universität, Klagenfurt
[**] Deptartment of Computer Systems Engineering, Quaid-e-Awam University, Nawabshah
[***] LIPADE, University Paris Descartes, Paris
[****] Department of Information Technology, Quaid-e-Awam University, Nawabshah

systems just need an image sensor with a built-in processing hardware for running image analysis.

The motivation of this research is based on our development of a small-scale, portable, image processing based system for detecting a driver's vigilance level. The proposed system uses a smart NIR camera to cope with the problem of changing light conditions. The algorithm proposed to perform driver's fatigue detection is based on detecting driver's eyes by using our (trained) Haar classifier and then detecting driver's iris using a template matching scheme. Our minimum hardware (a single smart camera comprising 1 GHz ARM Cortex A8 processor and 512 MB RAM) and the computationally-efficient algorithm provide a good potential of implementing our system in real scenarios.

The contribution in this paper is summarized as follows:

1 We performed an analytical survey on the existing methods of driver's fatigue detection and highlight their limitations.
2 We trained two detectors based on Haar features to detect the driver's face and then eyes within a region of interest.
3 We proposed a template matching algorithm for tracking the driver's iris within the detected eye and obtain statistics of the iris detection frequency and the direction of driver's gaze. We used this information to determine the driver's attention level and to generate an alarm in case of declined vigilance level.
4 We have completely implemented our algorithm on our selected hardware and performed long-term experiments in real scenarios to demonstrate the effectiveness of the algorithm.

The rest of the paper is structured as follows. In section 2, we provide an extensive survey and critical analysis of the existing approaches for driver's fatigue detection. Section 3 gives a detailed insight into the theoretical background of Haar features and describes the method of data collection and preparation for training a Haar classifier for face and eye detection. Section 4 describes the method of AdaBoost training for generating a trained classifier and section 5 provides details of iris detection with template matching. Section 6 presents the overall algorithm with the evaluation results. Section 7 concludes the paper with a potential future work.

2. RELATED WORK

The existing approaches for Driver's Fatigue Detection (DFD) can be broadly classified into three categories: (i) Studying the driver's mental state pertaining to driving safety by psychologists and real-time monitoring of several physiological conditions, e.g., brain frequency, heartbeat, pulse beat rate, rate of respiration, etc [3]; (ii) Devising auxiliary equipments for improving driving safety by designing special car seats, monitoring grip force change on the steering wheel, or analyzing EEG recordings from sensors attached to the human body [4]; (iii) Computer vision techniques to monitor the driver's expressions. Figure 1 depicts the classification of the existing techniques for determining driver's vigilance level.

2.1. PSYCHOLOGICAL AND PHYSIOLOGICAL ANALYSIS

Analyzing driver's physiological conditions [5][6][7] deliver the most accurate results. Measuring different psychological and physiological conditions such as brain frequency, heartbeat, pulse-beat rate, respiration rate, facial expressions, body postures, and head nodding, etc provide adequate information to determine the driver's attention towards driving. However, getting all these measurements is not straightforward, cost-effective and nonintrusive. It requires a set of special sensors and hardware to be worn by the drivers which causes annoyance for most of the people. Hence these techniques are not practically acceptable [8].

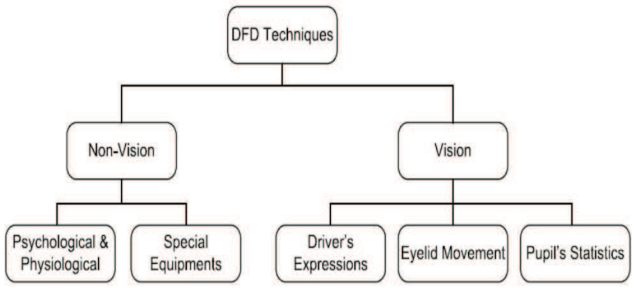

Fig. 1: Classifications of DFD Systems

2.2. SPECIALIZED VEHICLES

Some techniques for driver's fatigue detection use special vehicles with a number of sensing and processing elements installed in the vehicle to observe driver's

control over the vehicle [9][10][11]. The specialized hardware used in these vehicles include electroencephalogram, devices to send a visual stimulus to the driver and receiving a stimulus-response, and the sensors to monitor the steering wheel angle and the lateral position, etc. The information obtained from the sensing hardware includes steering wheels movements, acceleration, braking, lateral position and gear changing, etc. This information is continually processed by the processing hardware to determine the level of driver's control over the vehicle. While these techniques deliver an optimal level of performance and accuracy, they are limited to vehicle type and driving conditions [12].

2.3. COMPUTER VISION

Image processing techniques are the most flexible and cheaper solution for driver's fatigue detection. Several computer vision techniques for driver's fatigue detection are studied in the literature. The technique proposed in [13] uses cascades of classifiers to detect driver's mouth and the yawning expressing. The classifiers are trained to detect mouth and yawning and used in real-time to detect yawning expressing in successive video frames. A drawback of this approach is that the driver may not necessarily yawn when he is tired. Therefore, this technique is limited to a specific psychological behavior.

The approaches proposed in [14][15] are based on the statistics of eyelid movement. In these methods, the face area is segmented from the image based on a mixed skin tone model. The process of crystallization is simulated to obtain the location of eyes within face area. Later, eye area, average height of the pupil and width-to-height ratio are used to analyze the eye's status. Finally, the driver fatigue is confirmed by analyzing the changes of eye's states. Nevertheless, the eyelid statistics used in these approaches cannot be used in a generalized way for people belonging to diverse races and having diverse eye shapes.

Another approach presented in [16] first locates the driver's face by a Haar features based object detection algorithm. The driver's eye is detected and eyelid distance is computed. By analyzing the successive changes in eyelid distance over time, driver's fatigue can be detected and a warning can be issued. However, this approach shares the same limitations as in [14][15].

In another approach [17], the authors propose a real-time eye tracking based fatigue detection system that uses a dynamically generated eye template and exploits a correlation technique to detect the driver's eye. The frequency of eye blinking is calculated and a cross-correlation based classification technique is used to determine if the eye-blinking frequency is below a certain threshold and the driver should be warned. However, detecting eyes with template matching instead of a trained classifier results in high rate of false positives.

After a critical analysis of the existing DFD techniques, we can safely conclude that the non-vision based techniques are either expensive or are intrusive. On the other hand, the vision based DFD techniques proposed in the literature are either computationally expensive or have limited accuracy.

3. OUR WORK IN COMPARISON WITH RELATED WORK

We are committed to overcome the issues pertaining to existing vision-based DFD systems. For this purpose, we combine iris and head tracking in two different modules running in parallel so that the system is effective for the situations where the driver is wearing sun glasses. Instead of directly detecting driver's eyes and thus getting numerous false positives, we train and implement two classifiers for face and eyes detection which minimize the search space for iris tracking with template matching and help to avoid large number of false positives. In contrast to the existing approaches which mainly focus on the frequency of eye blinking or the open-eyes status in successive video frames, iris tracking also helps to detect driver's direction of gaze (straight, left, right, up, down) to determine his vigilance level. Our proposed algorithm is simple, computationally-efficient, robust and requires simple infrastructure. Our implementation hardware comprises a single NIR smart camera to overcome the problems related to different light conditions.

4. THEORETICAL BACKGROUND

Our face and eye detection algorithms are based on two (trained) Haar-classifiers adapted from [18]. Haar classifiers make use of Haar features which represent the unique set of an object's characteristics (face and eye in

our case) in an image and can be expressed by the concept of Haar wavelets [19].

Haar features perceive an image as a combination of small sub-images and represent the properties of individual sub-images. The set of features, in combination, reports the availability or non-availability of an object of interest within an image. For example, the separation between a black and a white region can be found by a bi-rectangular feature.

Using the features confined in rectangular areas, the authors in [20] propose summing up the pixel intensities within these regions to locate an object of interest in an image. Having an image database, the sum of the pixels corresponding to the region of an object of interest would be quite high and low for other objects of non-interest. For each object of interest, we can set a threshold value for pixel sum and compare the Haar features in a certain rectangular area with the threshold value. A pixel sum greater than the threshold value confirms the presence of an object of interest in an image [21]. This approach divides the image database into the images having objects of interest and those having different objects. Figure 2 shows the rectangular Haar features. A feature in this figure represents a scalar quantity calculated by summing up the pixels in the white region and subtracting those in the dark.

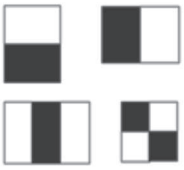

Fig. 2: Example rectangular Haar features

For each object in an image, there exists a unique set of features which represents the object classifier. There are two types of classifiers: *weak classifier* and *strong classifier*. A weak classifier, which performs naïve object detection, is obtained by subtractions of individual blocks computed within small rectangular regions of an image [22]. If a Haar feature is represented by *hj*, a weak classifier *wj(z)* for a certain threshold intensity T is defined as,

$$w_j(z) = \begin{cases} 1 & if\ p_j h_j(z) < p_j T_j \\ 0 & otherwise \end{cases}$$

where z is a sub-window in an image and p_j represents the direction of the inequality sign. A strong classifier $s(z)$ represents the combination of n weak classifiers and is defined as,

$$s(z) = sign\sum_{j=1}^{n} \alpha_j w_j(z)$$

Where α_j denotes the weight of a weak classifier $w_j(z)$ which is adjusted during the process of training strong classifier. The output of a strong classifier is 1 if the object of interest is found, or 0 otherwise. In order to train strong classifiers for face and eye detection, we use AdaBoost training [23] which finds optimal set of weak classifiers and further combines them into strong classifiers for face and eye detection. The AdaBoost training algorithm starts out with a binary labeled dataset of input feature vectors from the weak classifiers. In several rounds of learning, the weights of training samples are adjusted in order to correct the misclassifications. The convergence of the training algorithm results in a strong classifier which is the sum of the (correctly) weighted values of weak classifiers [23]. Figure 3 depicts the basic mechanism of AdaBoost training.

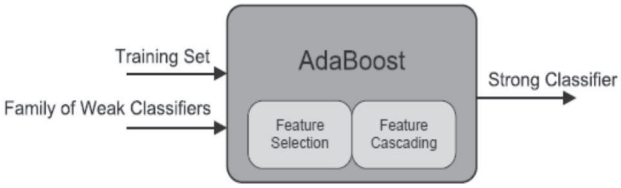

Fig. 3: Process of AdaBoost Training

5. TRAINING FACE AND EYE CLASSIFIERS

Before the AdaBoost training process, the first step involves collecting data (images) containing human faces and eyes. Two types of training samples are required: positive samples that contain the objects of interest, and negative samples that contain any type of objects other than the object of interest. We collected 2500 images each for training face classifier and eye classifier respectively from different online sources. Our image database contains images of the people from different nationalities and races. The collected data also contains 2500 negative

samples for each classifier. The example positive samples for face and eyes detection are shown in Figure 4.

Fig. 4a: Positive samples for face classifier

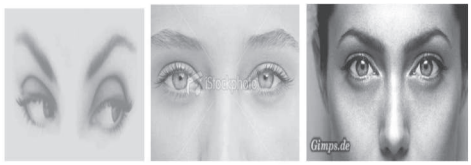

Fig. 4b: Positive samples for eye classifier

Fig. 4: Dataset for AdaBoost training

The next step includes labeling the faces and eyes in the images and cropping the images. We used an open-source utility [24] for labeling and cropping the images.

Once the dataset is ready, the next step involves feature selection from the labeled data, creating the weak classifiers and then using AdaBoost training to select the best weak classifiers and combine them into a strong classifier for both face and eye detection separately. For extracting face and eye features from the images and preparing data for AdaBoost training to generate a strong classifier, we used an OpenCV utility [25] to create training vectors comprising the face and eye feature values, respectively. This process generates 650 weak classifiers for face, and 629 weak classifiers for eye.

For AdaBoost training of face (strong) classifier, we create two sets each of *n* images: (i) the images having faces, (ii) the images having miscellaneous objects other than images. The same procedure is followed for training eye classifier with *n* images. The object and non-object images in both the cases are associated with the label O_i, where $O_i = \{1,0\}$. The AdaBoost algorithm for training a strong classifier with n weak classifiers is described in Algorithm 1. In this algorithm, z_n represents the nth training sample and O_n represents the object or non-object label.

ALGORITHM 1: AdaBoost training for face and eye classifiers

* ***Input:*** training data: $(z_1, O_1), \ldots, (z_n, O_n)$

* Specify training weights $\alpha_{1,i} = \frac{1}{2n_1}, \frac{1}{2n_2}$ where n_1 and n_2 represent the number of negative and positive samples, respectively.

* For every classifier indexed by $t = 1, \ldots, n$

* Normalize each weight with respect to the sum of all the weights, $\alpha_{t,i} = \frac{\alpha_{t,i}}{\sum_{j=1}^{n} \alpha_{t,j}}$

* Pick the classifier with the minimum error, $\delta_t = \min_{h,p,T} \sum_i \alpha_i \mid w(z_i, h, p, T) - O_i \mid$

* Set $w_t(z) = w(z, h_t, p_t, T_t)$ where h_t, p_t and T_t minimize δ_t

* Adjust weights: $\alpha_{t+1,i} = \alpha_{t,i} \gamma_t^{1-\mu_i}$ where $\mu_i = 0$ for correct classification, $\mu_i = 1$ for misclassification, and $\gamma_t = \frac{\delta_t}{1-\delta_t}$

* ***Output***: the strong classifier:

$$s(x) = \begin{cases} 1 & if \sum_{t=1}^{n} \log \frac{1}{\beta_t} w_t(x) \geq \frac{1}{2} \sum_{t=1}^{n} \log \frac{1}{\beta_t} \\ 0 & otherwise \end{cases}$$

Figure 5 shows the results of the final strong classifiers of face and eye detection. We tested the detectors on a large number of image database and found an accuracy of 99% and 98.5% for face and eye detection, respectively.

Fig. 5: Face and eye detection using the strong classifiers

6. IRIS TRACKING AND DETERMINING DIRECTION OF GAZE

We use a template matching technique for iris tracking and determining the direction of the driver's gaze. Given a sub-image (called template), the template matching technique tries to find the specified template within a large image. Template matching is an effective technique to find an object with fixed features and its position in an image. In our case, the template comprises a small pre-selected image of an iris. Since the shape of an iris does not vary significantly among different people, our template matching algorithm for iris tracking is not limited to specific physical characteristics. Once the driver's face and then eyes are detected, we have a very small search space in the image to match the iris template within the region of the detected eye. The small search space not only improves the speed of the template matching, but also helps to avoid false positives in case of low-light conditions or the presence of other similar features in the image.

Our template matching algorithm for iris tracking works as follows. We apply a template on a given image as a convolution mask and find the Sum-Of-Products (SOPs) of the neighboring pixels with the center pixel of the template. Starting with the left topmost pixel of the image, we move the template over the entire image and find the SOPs at each location. The SOPs and the template locations are temporarily stored in a look-up table. At the end of the search, all the SOPs are compared to find the one with the maximum value. The corresponding SOPs mark the location of the object (iris) in the image. Figure 6 shows the result of our template matching algorithm for iris tracking after face and eye detection.

Figure. 6: Iris tracking after face and eye detection

For speeding up the iris tracking, we prefer to detect only one eye. It is natural that if the driver feels sleepy, both the eyes will begin to close at the same time. By tracking iris, we can also determine the direction of gazing. The whole algorithm works in following steps:

The iris is detected within a specific rectangular area of the eye detection. Hence, we know the rectangular coordinates of the eye area. We also know the area surrounded by the iris and the coordinates of iris position returned by the template matching algorithm. With this information, we can compute the direction of gaze by comparing the iris coordinates with the eye coordinates. Figure 7 shows the bounding box of eye and relative position of iris from the coordinates of the eye's bounding box. The black circle represents iris's position while looking straight. The shaded circles represent iris's position while looking up, down, left or right. The parameters a,b,c,d represent iris's distance from the eye's bounding box while looking straight. Whereas a',b',c',d' represent iris's distance from the eye's bounding box while looking up, right, left and down, respectively. The direction of gaze is determined by comparing the iris's relative position with respect to the coordinates of the eye's bounding box. For example, if $a \leq a'$ the driver is looking upward.

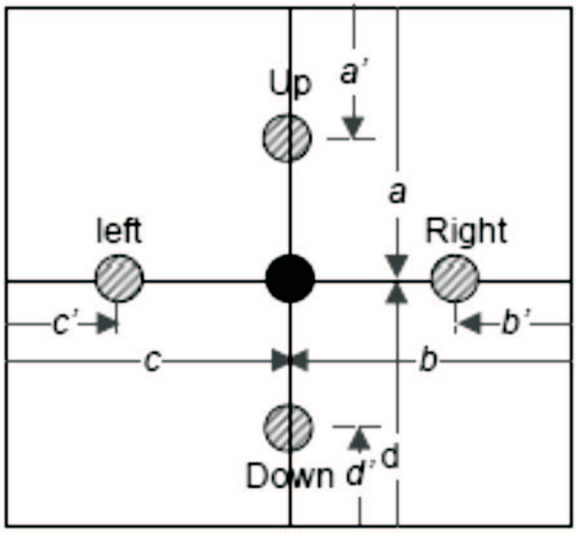

Figure. 7: Iris's relative distance from the eye's bounding box

Figure 8 shows the result of detecting direction of the driver's gaze. The directions mentioned in the figure are relative to the reader's view.

Figure 8a. Driver looking straight

Figure 8b: Driving looking left

Figure 8c: Driver looking right

Figure 8d: Driver looking up

Figure 8: Directions of driver's gaze determined by the iris tracking

The face detector also returns the head coordinates that are located at the upper part of the face's bounding box. This information is useful to track the head in situations where the driver is wearing sun glasses. At the startup, the algorithm obtains the current coordinates of the head from the face detector and updates these coordinates after regular intervals in time with the information obtained from the iris detection module. If the driver is sleepy, his head will begin to go down. Therefore, when required, the algorithm compares the head coordinates with the lower part of the image (bottom coordinates of the image) to check if there is a significant difference in the vertical coordinates. This situation is depicted in Figure 9. If the difference between the y coordinates of previous (head coordinates updated last time) and current bounding box is found to be equal to or greater than Δy, the head is assumed to be going down and a warning is generated. The steps involved in the algorithm are listed in Algorithm 2.

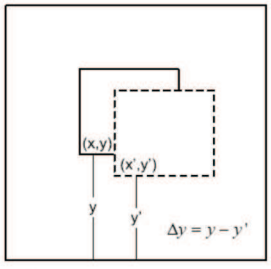

Figure 9: Difference of the last-updated and current head coordinates

ALGORITHM 2: Iris and head tracking

Start:

1. Detect driver's face
2. Track head for certain number of frames

2.1. If driver wearing glasses?

2.1.1. Update statistics of head coordinates.

2.1.2. Generate alarm on the basis of updated statistics

else

Go to step 3.

3. Detect driver's face

1. Detect driver's eye
2. Track iris by template matching

4.1. Determine direction of gaze

4.2. Determine frequency of iris

4.3. Update statistics of gaze direction and iris appearance

4.4. Generate alarm based on the updated statistics

4.4.1. If driver wearing glasses?

Go to step 2.

else

Go to step 3.

end.

7. OVERALL ALGORITHM AND EXPERIMENTAL RESULTS

Our experimental setup comprises a single NIR smart camera that not only has an image sensor to capture images, but is also capable of executing image processing tasks. The whole algorithm runs on the camera and the system does not require any additional processing hardware.

Our algorithm, running on the camera, starts with loading four modules, i.e., face detector, eye detector, head detector and iris tracker. At startup, the algorithm gets the head coordinates from the first instance of face detection. It then decides if the driver is wearing sun glasses by capturing and analyzing a certain number of images. If it doesn't detect eyes and iris for the next successive images, the algorithm assumes that the driver is wearing sun glasses and starts working with head tracking module only. Otherwise, for each new image, the algorithm first detects face and eye, and then makes sure that the iris is detected. It then determines the direction of gaze as mentioned in section 6. In case the iris is not detected or

the driver is not looking straight, the algorithm monitors the next successive images for 3 seconds to check if this situation persists. If the algorithm finds the same behavior in the next successive frames for 3 seconds, it generates an alarm. If the driver wears sun glasses during driving, the eye detector and iris tracker stop working for the next successive images. The algorithm again starts working with head tracking module only. Figure 10 and 11 show the results of fatigue detection and generating alarm. Our algorithm is able to process images at a speed of 20 frames per second.

Fig. 10: Iris tracking and alarm generation in case of iris disappearance for a certain amount of time

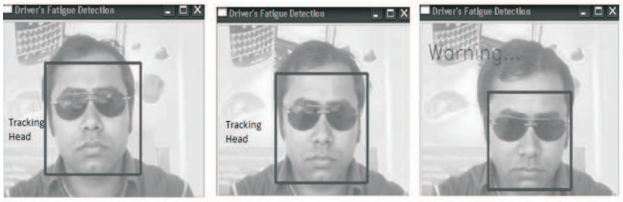

Fig. 11: Fatigue detection through head tracking and alarm generation

We tested our algorithm on a number of subjects at different times of the day under varying light conditions. During the test recordings, our subjects closed eyes on various occasions for a duration longer than a normal eye blink. We analyzed the impact of this behavior for false positives. The subjects were also asked to pretend to be sleepy in different ways. We noted down their behaviors and compared it with the alarms generated by our algorithm. Table I shows the results of our DFD algorithm.

	Test 1 (Afternoon)	**Test 2 (Evening)**	**Test 3 (Night)**
Total images processed	5000	5583	5760
Number of times eyes closed	15	18	20
Real sleep behavior	7	8	9
Alarms	7	8	8
False positives	0	0	1
False negatives	0	0	0
True positives	7	8	8
True negatives	0	0	0
Accuracy	100%	100%	88.9%
Average accuracy	95.8%		

Table 1: Evaluation results of the DFD algorithm

The results show that our algorithm is able to deliver an optimal accuracy. The only false positive detected in all the tests was during the experiment at night due to very low light.

8. CONCLUSION

In this paper, we have proposed a real-time driver's fatigue detection system based on iris tracking and (when required) head tracking. We constructed two detectors for eye and face detection. For iris tracking, we used a template matching based technique which speeds up the overall image processing pipeline. Before iris tracking, driver's face and eyes are detected and the search space is minimized for iris tracking. The statistics of iris tracking are continuously updated and if the iris tracker loses iris for a certain amount of time, the driver is assumed to be either wearing glasses or fatigued. In both the cases, an alarm is generated and a head tracking module is initialized which keeps track of driver's head and generates an alarm if the driver's head goes down below a certain threshold. In case the iris is tracked perfectly, but the driver is not found to be looking straight, an alarm is generated. Due to its simplicity and faster image processing with Haar-features based detectors and template matching, our system is capable of delivering an optimal performance with minimum hardware requirements.

Our future work in this direction includes image enhancement for extremely low-light conditions. The

image enhancement module incorporated to our DFD system will first analyze the contrast level of each image and determine if any enhancements are required. For this purpose, we are working on an adaptive and computationally-efficient image enhancement algorithm. Furthermore, we are also looking for migrating our algorithm on a camera having a dedicated Digital Signal Processor (DSP) for image processing which can further improve the speed of our algorithm.

REFERENCES

[1] Bergasa L.M., Nuevo J., Sotalo M.A., and Vazquez M., *Real-time system for monitoring driver vigilance*, In Proc. of Intelligent Vehicle Symposium, pp.78-83, 2004.

[2] Awake Consortium, *System for effective assessment of driver vigilance and warning according to traffic risk estimation (AWAKE)*, Sep. 2001–2004, [Online] Available: http://www.awake-eu.org.

[3] Qiang J., Zhiwei Z., and Lan P., *Real-time nonintrusive monitoring and prediction of driver fatigue,* In IEEE Trans. on Vehicular Technology, vol.53, no.4, pp. 1052- 1068, 2004.

[4] Horng, Wen-Bing et al, *Improvements of Driver Fatigue Detection System Based on Eye Tracking and Dynamic Template Matching*, In Trans. on Information Science and Applications, Issue 1, volume 9, 2012.

[5] Healey J., and Picard R., *SmartCar: Detecting driver stress*, In Proc. of 15th International Conference on Pattern Recognition, pp. 218–221, 2000.

[6] Kircher A., Uddman M., and Sandin J., *Vehicle control and drowsiness*, Swedish National Road and Transport Research Institute, Linkoping, Sweden, Technical Report VTI-922A, 2002.

[7] Anon, *Perclos and eyetracking: Challenge and opportunity*, Applied Science Laboratories, Bedford, MA, 1999, [Online] Available: http://www.a-s-l.com.

[8] Bergasa L.M., Nuevo J., Sotelo. M.A, Barea, R, Lopez, M.E., *Real-time system for monitoring driver vigilance*, In IEEE Trans. on Intelligent Transportation Systems, vol.7, no.1, pp.63-77, 2006.

[9] Artaud P., Planque S., Lavergne C., Cara H., Lepine P., Tarriere C., and Gueguen B., *An on-board system for detecting lapses of alertness in car driving,* In Proc. of 14th International Conference on Enhanced Safety of Vehicles, pp. 350-359, 1994.

[10] Mabbott N., Lydon M., Hartley L., and Arnold P., *Procedures and devices to monitor operator alertness whilst operating machinery in open-cut coal mines. Stage 1: State-of-the-art review*, ARRB Transport Res. Rep. RC 7433, 1999

[11] Lavergne C. et al, *Results of the feasibility study of a system for warning of drowsiness at the steering wheel based on analysis of driver eyelid movements*, In Proc. of 15th International Technical Conference on Enhanced Safety Vehicles, pp. 282-291, 1996.

[12] Ueno, H., Kaneda, M., Tsukino, M., *Development of drowsiness detection system*, In Proc. of Vehicle Navigation and Information Systems Conference, pp.15-20, 1994.

[13] Sarada D., Mandalapu, and Preeti B., *Driver fatigue detection using mouth and yawning analysis,* International Journal of Computer Science and Network Security vol. 8, no. 6, pp.183-188, 2008.

[14] Du, Yong, et al. *Driver Fatigue Detection based on Eye State Analysis*, In Proc. of the 11th Joint Conference on Information Sciences. pp. 1-6, 2008.

[15] Fan, Xiao, Bao-Cai Yin, and Yan-Feng S., *Yawning detection for monitoring driver fatigue*. In Proc. of IEEE Conference on Machine Learning and Cybernetics, pp. 664-668, 2007.

[16] Ma H., Yang Z., Song Y., and Jia P. *A Fast Method for Monitoring Driver Fatigue Using*

Monocular Camera. In Proc. of Joint Conference on Information Science, pp. 1-4, 2008.

[17] Khan M., and Mansoor A., *Real time eyes tracking and classification for driver fatigue detection*, In Proc. of conference on Image Analysis and Recognition, pp. 729-738, 2008.

[18] Viola P., and Jones M., *Rapid object detection using a boosted cascade of simple features*, In Proc. of IEEE Computer Society Conference on Computer Vision and Pattern Recognition, pp. 511-518, 2001.

[19] Stollnitz E.J., DeRose A.D., and Salesin, D.H, "*Wavelets for computer graphics: a primer.1*, In IEEE Trans. on Computer Graphics and Applications, vol.15, no.3, pp.76-84, 1995.

[20] Papageorgiou, Constantine P., Michael O., and Tomaso P., *A general framework for object detection.* In Proc. of IEEE Sixth International Conference on Computer Vision, pp. 555-562, 1998.

[21] Sang-Hyeon J., Kue-Bum L., Kwang-Seok H., *An implementation of multimodal Gaze Direction Recognition System using Image and EOG*, In Proc. of 6th International Conference on Digital Content, Multimedia Technology and its Applications (IDC), pp.229-234, 2010.

[22] Eng-Jon O., Bowden R., *A boosted classifier tree for hand shape detection*, In Proc. of Sixth IEEE International Conference on Automatic Face and Gesture Recognition, pp. 889- 894, 2004.

[23] [23] Viola P., and Michael J., *Robust real-time face detection*, International journal of computer vision vol. 57, no. 2, pp.137-154, 2004.

[24] http://sourceforge.net/projects/opencv /CV_TrainingPede.zip

[25] Bradski G., and Adrian K.., *Learning OpenCV: Computer vision with the OpenCV library*, O'Reilly Media, Incorporated, 2008.

[26] Figueiredo, Lino, et al. *Towards the development of intelligent transportation systems*. In IEEE Proceedings on Intelligent Transportation Systems, pp. 1206-1211, 2001.

[27] Khan, Umair Ali, and Bernhard Rinner. *A Reinforcement Learning Framework For Dynamic Power Management of a Portable, Multi-Camera Traffic Monitoring System.* In IEEE Proceedings on Green Computing and Communications (GreenCom), pp. 557-564, 2012.

ISSN 1605-8607

CHARACTERIZATION OF THERMAL EXPANSION OF THERMO-SET COMPOSITES

Fareed Hussain Mangi*, Asif Ali Memon**, Yasir Nawab

ABSTRACT

Use of composite materials in engineering applications has been increased significantly during the last decades due to their good mechanical properties despite lighter weight. A significant advantage of such materials is the choice of selection among several polymers and different types of reinforcement (fibre/fabric) types to achieve required properties. But this heterogeneous nature also induces several problems and makes thermo-mechanical behaviour complex. Thermal expansion of thermoset composite material is thus a parameter to know accurately. In laminated composites, this parameter depends largely on the orientation of plies, fibre fraction, type of resin and fibres, etc. In this article, some results on the determination of coefficients of thermal expansion (CTE) of composite plates (with stacking sequence 0, 0/90, 0/45, +/-45) at different angles in XY, XZ, and XYZ plane using finite element analysis and homogenized properties are presented. Experimental values of these coefficients for 0/90 stacking are found in agreement with the simulations. Finally, a mathematical model, based on strain matrix is proposed for modelling these coefficients.

Keywords : thermoset composites, liquid infusion moulding, thermal expansion, dilatometer

1. INTRODUCTION

Use of composite materials in engineering applications has been increased significantly during the last decades due to their good mechanical properties despite lighter weight [1]. Depending of type of end use different types of reinforcement e.g. unidirectional fibres, woven fabric, knitted, or braded fabrics, are used to achieve required properties in composite part [2]. The polymers used in composites are classified as: thermoset and thermoplastic ones. Thermosetting polymers e.g. epoxy, unsaturated polyester, and vinylester are commonly used in aerospace and naval applications due to their low viscosity, which makes easy the impregnation of reinforcement and hence process of fabrication.

Knowledge of thermal expansion and /or shrinkage is essential to characterize the behaviour of thermoset composite materials [3]. In case of laminated composites, the differences between the coefficients of thermal expansion of the constituents, i.e. fibres, matrix, and mould lead to the formation of residual stresses and deformations in the composite part [4-7]. Characterization of these coefficients is thus essential for modelling. Generally, it is considered that out of plane coefficient of thermal expansion (CTE) is equal to the transversal (in-plane) thermal coefficients [8].

In the present article, thermal expansion coefficient of a unidirectional glass/epoxy laminated composite plate was determined in different directions in the plane, and out of plane of the piece. It was found that the out of plane coefficients are not equal to the in-plane transversal coefficients, which is against the previously believed concept. Moreover, a significant effect of Tg was also observed on the thermal coefficients of the composite. These coefficients were also modelled using strain matrix and found in agreement with the experimental ones.

2. MATERIAL AND METHODS

In this study, a laminated composite plate (300 mm× 300

* Université de Nantes, CNRS, Laboratoire de Thermocinétique de Nantes, UMR 6607, La Chantrerie, rue Christian Pauc, BP 50609, 44306 NANTES cedex 3 – France (fareedmangi@gmail.com)

** Energy and Environment Engineering Department, Quaid-e-Awam university of Engineering, Science and Technology, Nawabshah

mm× 40 mm) was fabricated using vacuum assisted resin transfer moulding (VARM) such as the fibre volume fraction is equal to 50%. All the plies were stacked at zero degree. The polymerization was carried out at room temperature.

Parallelepiped samples (10mm× 10mm× 30-40mm) were cut into the composite plate, in directions defined by a direction coefficient 0 or 1, according to the axis X, Y and Z: (1,0,0), (0.1 , 0), (0,0,1), (1,1,0), (0,1,1), (1,0,1) and (1,1,1). To determine the CTE, a classical dilatometer was used. Samples are given names (Table 1) for easy understating.

Table: Samples names and corresponding orientations

Name	S1	S2	S3	S4	S5	S6	S7
Orientation	100	010	001	110	101	011	111

For determination the Tg of composite, a differential scanning calorimeter (DSC Q200-TA instruments) was used.

2.1. DIFFERENTIAL SCANNING CALORIMETER

This technique has been used to identify heat of cure, specific heat capacity, glass transition temperature (Tg) and degree of cure (α) of polymer [9]. Differential Scanning Calorimeter (DSC) consists of two cells called reference and sample cell. During the heating, it measures the difference of heat that is consumed by sample as compared to the reference, for reaching a given temperature. The instrument used in our study was a DSC Q200 from TA instruments.

2.2. DESCRIPTION OF DILATOMETER

DI.24 ADAMEL LHOMARGY® is the dilatometer, which was used for the thermal expansion measurements of composite samples. It consists of an oven, an aluminium support, thermocouples, and LVDT sensors.

1. The oven consists of a heater based on the silicon carbide resistor, which can heat the sample from room temperature to 1600°C. The oven can be moved on a rail to facilitate the sample placement.
2. Silicon support, for placing the samples of dimensions 10 to 50 mm long in the oven. The cross-section of sample can be up to 10mm x10mm.
3. Two thermocouples are employed, one in the silicon support for the measurement of sample temperature, and second in the centre of the oven to control the heating temperature.

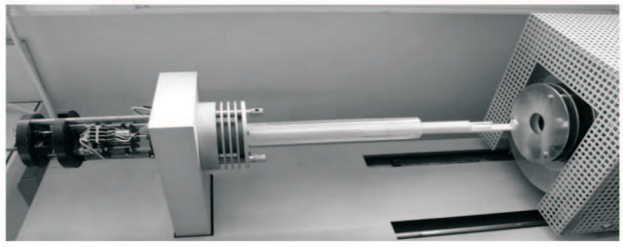

Figure 1: DI.24 (ADAMEL LHOMARGY ® dilatometer

The head consists of a LVDT (Linear variable differential transformer) type displacement sensor, and two screws for adjusting the zero and initial load on the sample. The sample placed on aluminium support is hold with a pressing bar. This bar can be positioned with two screws to adjust zero strain and initial pressure on the sample (1mm in our case). This bar is linked to the LVDT sensor. The length variations during the heating/cooling ramps are then recorded. The precision of used instrument is +/- one micrometer.

3. RESULTS AND DISCUSSION

3.1. DETERMINATION OF TG

Glass transition temperature (Tg) is the temperature at which polymer converts from glassy state to rubbery state or vice versa. This temperature has a significant effect on thermo-mechanical properties of polymers and polymer reinforced composites. Therefore, it is an important factor to find out. In the present paper, differential scanning calorimeter was used to characterize Tg of glass/epoxy composite samples. 10-15 gram of composite sample were sealed in aluminium hermetic pan and scanned for the temperature range of 0°C -100°C at the heating rate of 4°C/min. The average value of Tg was found equal to 56 ± 2 °C.

3.2 DETERMINATION OF THERMAL COEFFICIENTS

In order to determine the thermal coefficient, samples were submitted to the following thermal cycle:

1. Heating from room temperature to 100°C at the rate of 2°C/min
2. Cooling to 20°C at rate of 2°C/min

3. Maintaining at 20°C for 80 min

This cycle was repeated 2-3 times for a sample. For each orientation, two samples were tested, and then average of both results was taken as the final results.

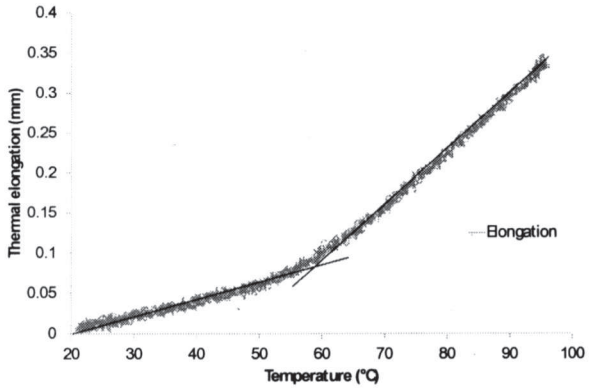

Tg

Figure 2: Thermal elongation versus temperature response of samples 011

In Figure 2, Elongation response of composite sample 011(diagonal in xz plane) during the heating step is plotted versus temperature. Slope of a graph is directly proportional to the coefficient of thermal expansion, which can be found using the simple expression: $CTE = \frac{1}{e_0}\left(\frac{\partial e}{\partial T}\right)$, where e_0 is the initial length of the sample, T is the temperature, and e is length at this temperature.

The elongation versus temperature curve can be divided into two linear zones in figure 2. The first one starts from room temperature to the temperature of 56-58°C. In this zone composite was in the glassy state. Therefore, slope of the graph of this portion when divided by sample length will result into CTEglassy. Whereas, the slope of second linear portion after divided by sample length will result into CTE of composite in rubbery state. This change of slope occurs in the zone of glass transition of composite sample (56 ± 2 °C found by DSC). Therefore, it can be concluded that the change in slope is due to glass transition from glassy to rubbery state.

Figure 3 shows the comparison of CTEs below Tg of all the tested samples. It can be noted that CTE of the sample S_1 (along the fibres direction) is minimale (6.1×10^{-6} K^{-1}). The value of CTE in transversal direction (S_2) is higher than the value of CTE through the thickness (S_3). This result was surprising but several repetitions on samples from different composite parts gave the same results which lead us to conclude that this result is correct.

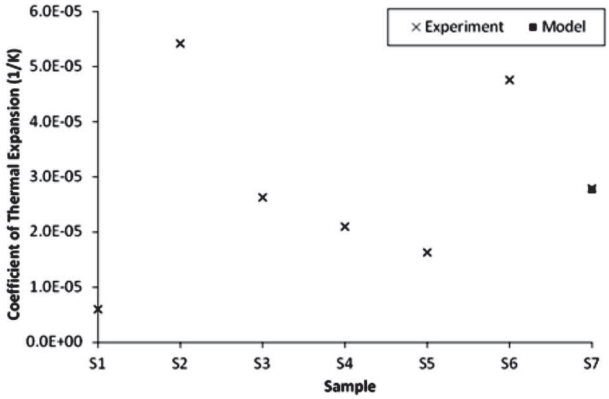

Figure 3: Linear coefficients of thermal expansion (1/K)

CTE of sample S_5 (diagonal in xz plane) has lesser value as compared to other diagonal samples (S_4, and S_6), which is normal because no component of CTE along y-axis was included in this coefficient. CTE of samples S_7 was found approximately equal to CTE along z-axis.

The next step was to propose a model for CTE, depending on angle of orientation of fibres. At first, an attempt was made to use strain matrix to calculate the CTE_{111} (of a sample in space making 45° with its projection in xy plane) from the experimental values of other six CTEs, which was then compared with the experimental value. The strain ε_{xyz} (denoted by ε in equation below) is given by the matrix:

$$\vec{\varepsilon}\vec{m} = \begin{bmatrix} \frac{\varepsilon_{xx}}{\sqrt{3}} + \frac{\varepsilon_{xy}}{\sqrt{3}} + \frac{\varepsilon_{xz}}{\sqrt{3}} \\ \frac{\varepsilon_{xy}}{\sqrt{3}} + \frac{\varepsilon_{yy}}{\sqrt{3}} + \frac{\varepsilon_{yz}}{\sqrt{3}} \\ \frac{\varepsilon_{xz}}{\sqrt{3}} + \frac{\varepsilon_{yz}}{\sqrt{3}} + \frac{\varepsilon_{zz}}{\sqrt{3}} \end{bmatrix} \begin{bmatrix} \frac{1}{\sqrt{3}} \\ \frac{1}{\sqrt{3}} \\ \frac{1}{\sqrt{3}} \end{bmatrix}$$

For one degree rise in temperature (2.1) can be written as

$$CTE_{111} = \begin{bmatrix} \frac{CTE_{100}}{\sqrt{3}} + \frac{\varepsilon_{xy}}{\sqrt{3}} + \frac{\varepsilon_{xz}}{\sqrt{3}} \\ \frac{\varepsilon_{xy}}{\sqrt{3}} + \frac{CTE_{010}}{\sqrt{3}} + \frac{\varepsilon_{yz}}{\sqrt{3}} \\ \frac{\varepsilon_{xz}}{\sqrt{3}} + \frac{\varepsilon_{yz}}{\sqrt{3}} + \frac{CTE_{001}}{\sqrt{3}} \end{bmatrix} \cdot \begin{bmatrix} \frac{1}{\sqrt{3}} \\ \frac{1}{\sqrt{3}} \\ \frac{1}{\sqrt{3}} \end{bmatrix}$$

The values ϵ_{xy}, ϵ_{yz}, ϵ_{xz} can be found by solving the strain matrices in their respective planes. By solving (2.2), the value of CTE_{111} was found equal to 2.79×10^{-5} K^{-1} .The experimental value ranges from 2.77×10^{-5}. The results show that a mathematical model based on above approach may be suitable for such estimations. Model can be improved by considering the other thermophysical phenomena such as Tg, etc.

CONCLUSION

In the present study, effect of fibre orientation on thermal expansion of glass/epoxy unidirectional laminated composite is studied. It was observed that Tg has a significant effect on CTE of composite. It is found experimentally, that CTE is minimum along the fibres in XY plane. Value of CTE, when taken out of plane, increases with angle and reaches maximum value along the Z-direction (out of plane). As a whole, value of thermal coefficient along Y-axis was the greatest among other directions in the composite part. More experiments at different orientations are required to propose a comprehensive mathematical model.

REFERENCES

[1] Reddy JN. Mechanics of laminated composite plates and shells: theory and analysis. 2nd ed: CRC Press, USA; 1945.

[2] Nawab Y, Legrand X, Koncar V. Study of changes in 3D-woven multilayer interlock fabric preforms while forming. Journal of The Textile Institute. 2012;103(12):1273-9.

[3] Parlevliet PP, Bersee HEN, Beukers A. Residual stresses in thermoplastic composites - a study of the literature. Part III: Effects of thermal residual stresses. Composites Part A: Applied Science and Manufacturing. 2007;38(6):1581-96.

[4] Yoon KJ, Kim J-S. Effect of Thermal Deformation and Chemical Shrinkage on the Process Induced Distortion of Carbon/Epoxy Curved Laminates. Journal of Composite Materials. 2001;35(3):253-63.

[5] Yates B, McCalla BA, Sargent JP, Rogers KF, Phillips LN, Kingston-Lee DM. The thermal expansion of carbon fibre reinforced plastics. J Mater Sci. 1978;13(10):2217-25.

[6] Peeters LJB, Powell PC, Warnet L. Thermally-Induced Shapes of Unsymmetric Laminates. Journal of Composite Materials. 1996;30(5):603-26.

[7] Nawab Y, Jacquemin F, Casari P, Boyard N, Sobotka V. Shape evolution of carbon epoxy laminated composite during curing," Key Engineering Materials. Key Engineering Materials. 2012;504-506:1145-50.

[8] Gay D, Hoa SV, Tsai SW. Composite materials : Design and Applications: CRC Press; 2003.

[9] Schick C. Differential scanning calorimetry (DSC) of semicrystalline polymers. Analytical and Bioanalytical Chemistry. 2009;395(6):1589-611.